8-2-2003

Surface Characterization of Rh-Co, Ru-Co and Pd-Co Bimetallic Catalysts

Sajeev Moorthiyedath

SURFACE CHARACTERIZATION OF Rh-Co, Ru-Co, and Pd-Co BIMETALLIC CATALYSTS

By

Sajeev Moorthiyedath

A Thesis
Submitted to the Faculty of
Mississippi State University
in Partial Fulfillment of the Requirements
for the Degree of Master of Science
in Chemical Engineering
in the Dave C. Swalm School of Chemical Engineering.

Mississippi State, Mississippi

August 2003

SURFACE CHARACTERIZATION OF Rh-Co, Ru-Co, and Pd-Co

BIMETALLIC CATALYSTS

By

Sajeev Moorthiyedath

Approved:

Kirk H. Schulz Earnest W. Davenport Jr. Chair and Director of Dave C. Swalm School of Chemical Engineering (Major Professor)	Clifford E. George Professor of Chemical Engineering (Committee Member)
Hossein Toghiani Associate Professor of Chemical Engineering (Committee Member)	Priscilla J. Hill Assistant Professor of Chemical Engineering (Committee Member)
Mark E. Zappi Texas Olefin Professor and Graduate Coordinator of Chemical Engineering	A. Wayne Bennett Dean of Bagley College of Engineering

Name: Sajeev Moorthiyedath

Date of Degree: August 2, 2003

Institution: Mississippi State University

Major Field: Chemical Engineering

Major Professor: Dr. Kirk H. Schulz

Title of Study: SURFACE CHARACTERIZATION OF Rh-Co, Ru-Co, and Pd-Co BIMETALLIC CATALYSTS

Pages in Study: 118

Candidate for Degree of Master of Science

Methanation of CO_2, a greenhouse gas component, using bimetallic catalysts is considered. Rh, Pd and Ru were combined separately with Co on silica support to form bimetallic catalysts with 5 % metal loading and atomic ratio to Co equal to 1. Pore volume of the silica was measured using physisorption analysis. The unreduced catalyst samples were characterized using XPS, TPR and SEM-EDS.

XPS results showed low Rh, Pd, Ru and Co concentrations at the surface for the three bimetallic catalysts. The oxidation states of metals detected by XPS supported the likely presence of metals in their oxide form. Detection of alloys and/or bimetallic particles on the surface of the catalysts was difficult through the XPS results, but presence of bimetallic particles was confirmed in Ru-Co and Pd-Co catalysts through the TPR results. Surface segregation of cobalt was observed. This was supported and extended to other metals through the SEM-EDS results.

DEDICATION

I dedicate this thesis to my beloved parents.

ACKNOWLEDGEMENTS

First of all I would like to thank Dr. Kirk Schulz, my advisor and major professor for his help, guidance and support throughout the course of this research and during my program of study here at MSU. I also would like to thank Dr. Hossein Toghiani for the enormous time and effort that he spent guiding and helping me during the course of this project. My sincere acknowledgements also go to the committee members, Dr. Clifford George and Dr. Priscilla J. Hill. I also would like to thank Dr. Rebecca Toghiani and Dr. Mark E. Zappi, the Graduate Coordinators during my Masters program in the Chemical Engineering Department. A very special note of thanks goes to Venkata Ramesh Chilukuri, for his sincere help during the experimentation of my thesis. I also would like to thank the Surface Science group of Esteban Romano, Holly Martin and Melissa Graves for their help in the XPS experiments. Acknowledgements also go to Richard F. Kuklinsky and Bill Monroe for their help in SEM analysis and to Dr. Qiangu Yan for his help in the thesis as well. I would also like to thank the Dave C. Swalm School of Chemical Engineering for the financial support throughout my thesis. Last but not the least, I would like to thank my family and friends for their continuous encouragement during the course of my study here in Mississippi State University.

TABLE OF CONTENTS

CHAPTER Page

LIST OF TABLES

TABLE Page

LIST OF FIGURES

FIGURE Page

CHAPTER I

INTRODUCTION AND BACKGROUND

Global emissions are rising, and unless the government puts in control measures, they will not subside. The increase in the concentration of greenhouse gases, namely, carbon dioxide, methane and Chlorofluorocarbons, are mainly from the combustion of fuels, industrial pollution, agriculture, and forestry, etc. Figure 1.1 shows percentage emissions of greenhouse gases (GHG) from human activity. So what are the chances of stopping these greenhouse gas emissions? [1].

The Kyoto protocol is one promising international convention adopted by 160 countries worldwide in December 1997. The agreement requires 38 industrialized countries to reduce the emissions of six major greenhouse gases by 5.2 percent during the 2008-2012 period. This convention has the objective of maintaining the concentration in the atmosphere of the Greenhouse house gases at an optimum level [1].

If one compares the level of emissions in 1990 with emissions today, there has been a significant percentage increase in the emissions of the major greenhouse gases in the U.S, which is the world's largest emitter. [Table 1.1]. Additionally, the level of carbon emissions is expected to be 33 percent larger in 2010 than in 1990 [1].

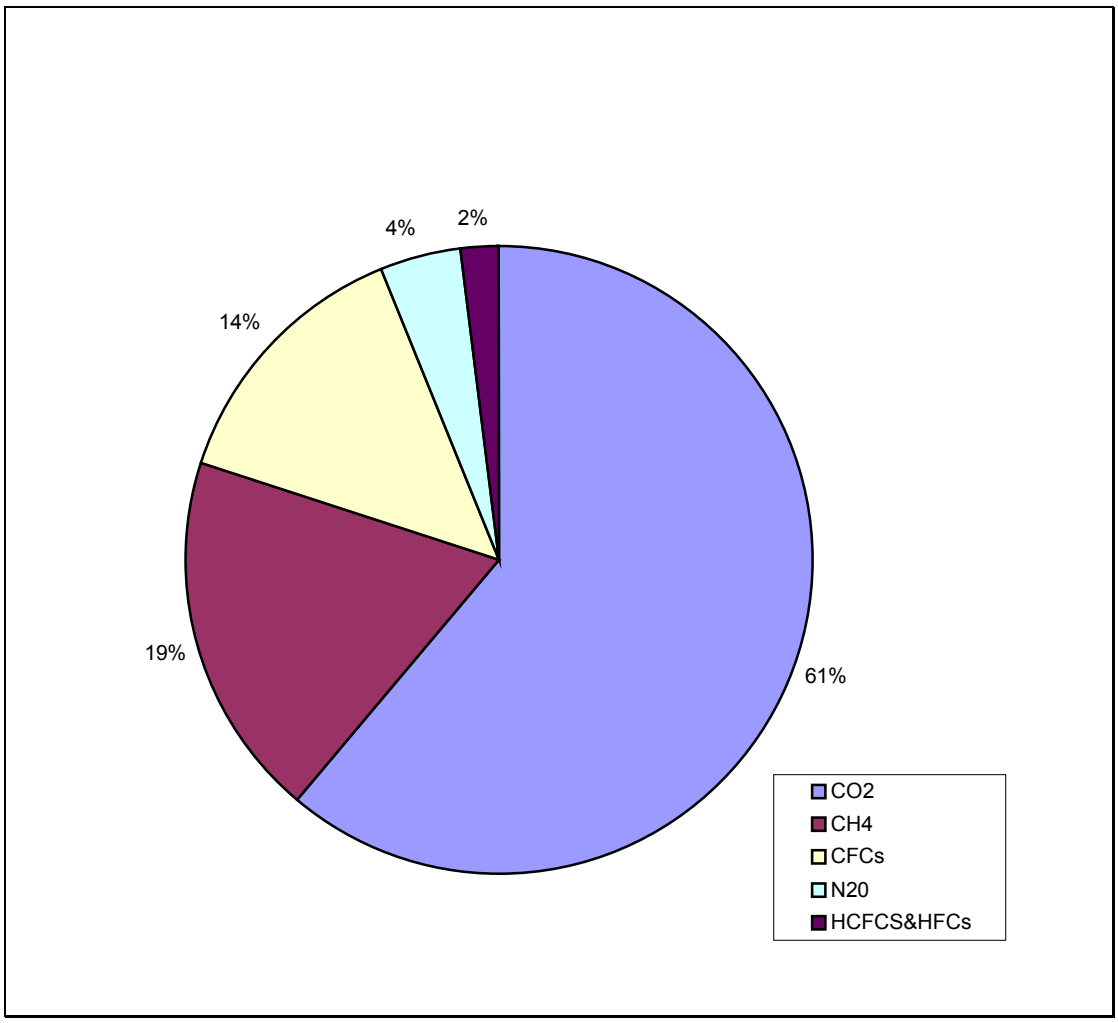

Figure 1. 1 Percentage emissions of Greenhouse Gases from human activity

Table 1. 1 U.S emissions of Green House Gases during 1990-1999 based on Global Warming potential [2]
(Million Metric Tons of Carbon Equivalent)

GAS	**1990**	**1995**	**1997**	**1999-P**
CARBON DIOXIDE	1,351	1,435	1,505	1,527
METHANE	182	179	172	165
HFC's, PFC's, and SF6	24	29	35	38
NITROUS OXIDE	99	106	104	103
TOTAL	1,655	1,748	1,816	1,833

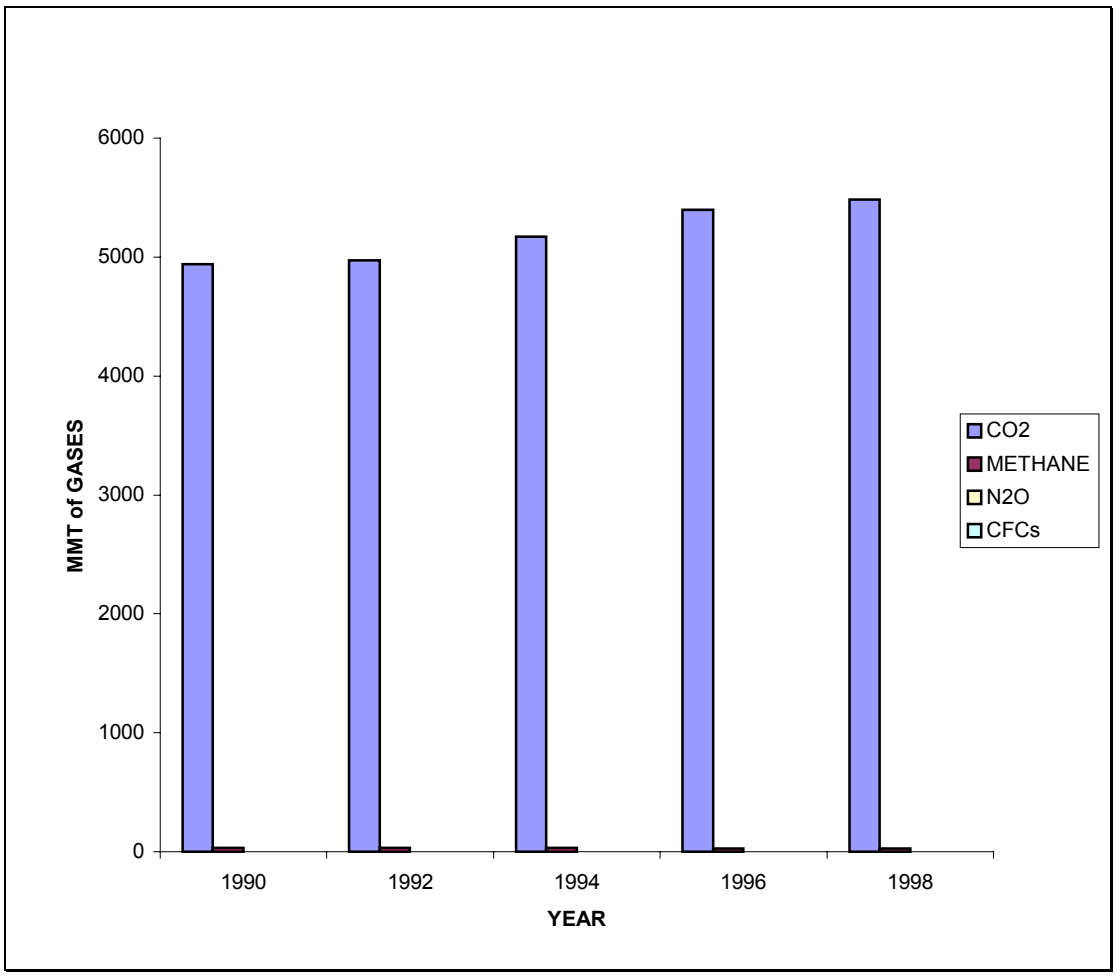

Figure 1. 2 Carbon dioxide emissions in MMT over a ten-year period in the US

Sources of carbon dioxide emissions

Emissions of carbon dioxide from industries resulting from combustion of fossil fuel and from electric utilities have resulted in a 33 percent increase in these emissions [3]. In 1999 about 31 percent of the carbon dioxide emissions came from the transportation sector. Most of these came from petroleum products, two-thirds from fuel combustion in motor vehicles and the rest from others like jet fuel in aircraft [2].

Emissions estimates suggest a sharp increase in carbon dioxide emissions from energy use in the United States by 2010 [4]. Emissions of CO_2 were 5169.7 MMT in 1994 (Figure 1.2), and increased about 300 MMT over the next four years [5]. IPPC records suggest that global average temperatures will eventually rise by between 1.5^0 C and 4.5 deg C if carbon dioxide concentrations double. If this happens, the global warming would be greater than anything experienced so far [6].

If the emissions of carbon dioxide are maintained at their present level, then there is a possibility that CO_2 in the atmosphere could double by 22^{nd} century. Emissions would have to decrease to less than 30 percent of the current levels if concentrations are to be maintained at doubled CO_2 levels around the 22^{nd} century [7]. The ice during the summers in the Artic region could decrease by 60%, if the level of CO_2 doubles [8]. From the view -point of global environmental protection, recycling of fossil fuel through catalytic hydrogenation of carbon dioxide is attracting great attention.

Table 1.2 Sources of carbon dioxide emissions [2]

Stationary Sources	**Mobile Sources**	**Natural Sources**
Fossil Fuel-based Electric Power Plants	Automobiles and Sports Utility Vehicles	Humans
Independent Power Producers	Trucks and Buses	Animals
Manufacturing Plants in Industry	Aircraft	Plant and Animal Decay
Commercial and Residential Buildings	Trains and ships	Land Emission/leakage
Flares of Gas at Fields	Construction vehicles	Volcano
Military and Government Facilities	Military Vehicles and devices	Earthquake

Solutions to carbon dioxide reductions

With a view to solving this problem, researchers have been investigating possible CO_2 reduction options. Methods ranging from CO_2 capture by pre-combustion decarbonization of natural gas [9] to biologically enhanced recovery of carbon dioxide [10] have been suggested. NASA is looking for new methods of carbon dioxide conversion to fuels as part of possible manned missions to Mars [11]. Additionally, photo catalytic [12] and photo-reduction [13] mechanisms have also been suggested to convert CO_2 into useful products, thereby reducing CO_2 emissions.

One proposed method of CO_2 reduction is 'carbon dioxide sequestration'. The process of carbon sequestration has focused mainly on three different approaches.

- CO_2 capture and separation.
- Dumping of the carbon dioxide into the ocean to provide phytoplankton growth.
- Improved chemical, biological and decarbonization methods.

One promising approach is to convert CO_2 into useful products such as hydrocarbons or alcohol fuels. The Carnol Process is a useful method to reduce the CO_2 from the power plants. It utilizes the three basic steps:

1. Carbon-dioxide extraction from the flue gases of the coal fired power plants using monoethanolamine (MEA) solvent in an absorption-stripping operation.
2. The production of hydrogen by the thermal decomposition of methane to carbon and hydrogen as given: $CH_4 = C + 2H_2$
3. The third step in this process is reacting hydrogen with the CO_2 from the step1 and is given by the equation $CO_2 + 3H_2 \rightarrow CH_3OH + H_2O$

4. This is an exothermic reaction so that the heat produced in this reaction can be use to recover the CO_2 from the absorption/stripping operation in step1.

Hence, catalytic hydrogenation of CO_2 is gaining in importance, partly because it is fast and efficient compared to other chemical process such as bio-chemical /enzymatic conversion, solar-thermal/catalytic conversion, photochemical/catalytic conversion etc. Initial studies were based on hydrogenation on metal supported catalysts. Methanol is one useful product of carbon dioxide conversion. The usefulness of this reaction occurs because methanol can be used as an alternative fuel, in internal combustion (IC) engines with reduced CO and HC emissions. Methanol can be used either directly or indirectly in fuel cells at several times higher conversion efficiency for automotive use. A great advantage of methanol is that, as a liquid, it fits in well with the infrastructure of storage and distribution compared to compressed natural gas and gaseous or liquid hydrogen, which are also being considered as alternative transportation fuels [2]. Additionally methanol can be used as a chemical component of the fuel additive MTBE (Methyl tertiary butyl Ether) and TAME (Tertiary Amyl Methyl Ether).

The methanol production industry generates approximately $12 billion in economic activity. Additionally, is a building block for other chemicals. Methanol is one of the key petrochemicals with a worldwide annual production of almost 30 million tons [14]. Methanol can be used to synthesize formaldehyde, acetic acid, chloromethanes, methylamines and various miscellaneous chemicals. Other uses of methanol include use as a solvent, antifreeze, inhibitor in natural gas processing, and substrate for crop growth and sewage treatment. Furthermore since storage and transportation is not a problem with

methanol, its synthesis from hydrogen and carbon dioxide can reduce the problem of hydrogen storage in the future energy scenarios [13].

Methanol synthesis from CO_2 on Cu/ ZnO catalysts [15] has received significant attention. Practical methanol production processes require good performing catalysts. Attaining high selectivity catalysts is the major problem in converting carbon dioxide to methanol. The challenge lies in finding a catalyst highly selective to methanol with low selectivity to CO production, which is formed via the reverse-water-gas shift reaction [13] Additionally, catalyst activity and selectivity must be high for a long operational period [14]. Group VIII elements play a vital role towards this process. Elements like Rh, Co, Ni, and Pd serve as important catalysts for CO_2 hydrogenation.

Bimetallic catalysts

Methanation has the following basic reaction:

$$CO_2 + 3H_2 \rightarrow CH_3OH + H_2O$$

This involves the catalytic hydrogenation of CO_2 at elevated temperatures of 500-600 K and pressures of 5 Mpa, respectively [16]. Thus we find from the literature that several catalysts (both metallic and bimetallic) were used towards this type of reaction with a focus on the bimetallic group VIII, IX and X metals.

Bimetallic catalysts have been the subject of study for the past three decades. Bimetallic catalysts are effective due to the interaction between the two metals, which leads to the improvement in both the activity and selectivity of the catalysts. Catalysts are classified as 'monometallic' or 'bimetallic', depending on the number of transition metals present in the particular catalyst in their metallic or oxidized state. This interaction between the two metals is due to the physical promotion provided by either of the metals or by the transfers of electron from one metal site to the other [17].

Bimetallic systems exhibit intriguing catalytic properties, particularly the group VIII, IX and X elements. Figure 1.3 shows a typical example of the importance of addition of one bimetal with the other in ethane hydrogenolysis and cyclohexane dehydrogenation [18]. When nickel is alloyed with copper in catalysts used for such reactions of hydrocarbons as in ethane hydrogenolysis and cyclohexane dehydrogenation, the effect of the addition of copper on the catalytic activity depends on the type of reaction. The addition of a small amount of copper to nickel actually increases the catalytic activity several times. Further addition of copper to about eighty percent pure

copper has very little effect [17]. The catalytic activity decreases sharply when pure copper is used as the catalyst. In situations where a molecule can undergo several different reactions, bimetallic catalysts often remove unwanted reactions and therefore maximize desired reactions.

Bimetallic clusters

A bimetallic entity with a large fraction of its atoms in the surface is known as a bimetallic cluster. These bimetallic clusters better define the type of activity that takes place in catalysis. John H. Sinfelt was the first person to clearly illustrate the arrangements of these clusters and to find their typical diameters. Thus, pairs of bimetallic elements that do not form alloys in nature have been found to form bimetallic clusters. These bimetallic clusters usually constitute around one percent of the total catalyst mass, [21] which is the percent metal dispersion. Catalysts containing these bimetallic clusters are used in petroleum refining, particularly in the production of gasoline with "superior anti-knock" properties. Also they are also used in reforming operations, where they have the ability to maintain their activity for a much longer time. In general, bimetallic catalysts make use of the group VIII, IX and X metals as primary catalysts and are used for hydrogenation reactions. These elements are particularly effective when compared to elements of other group during hydrogenation and hydrogenolysis reactions.

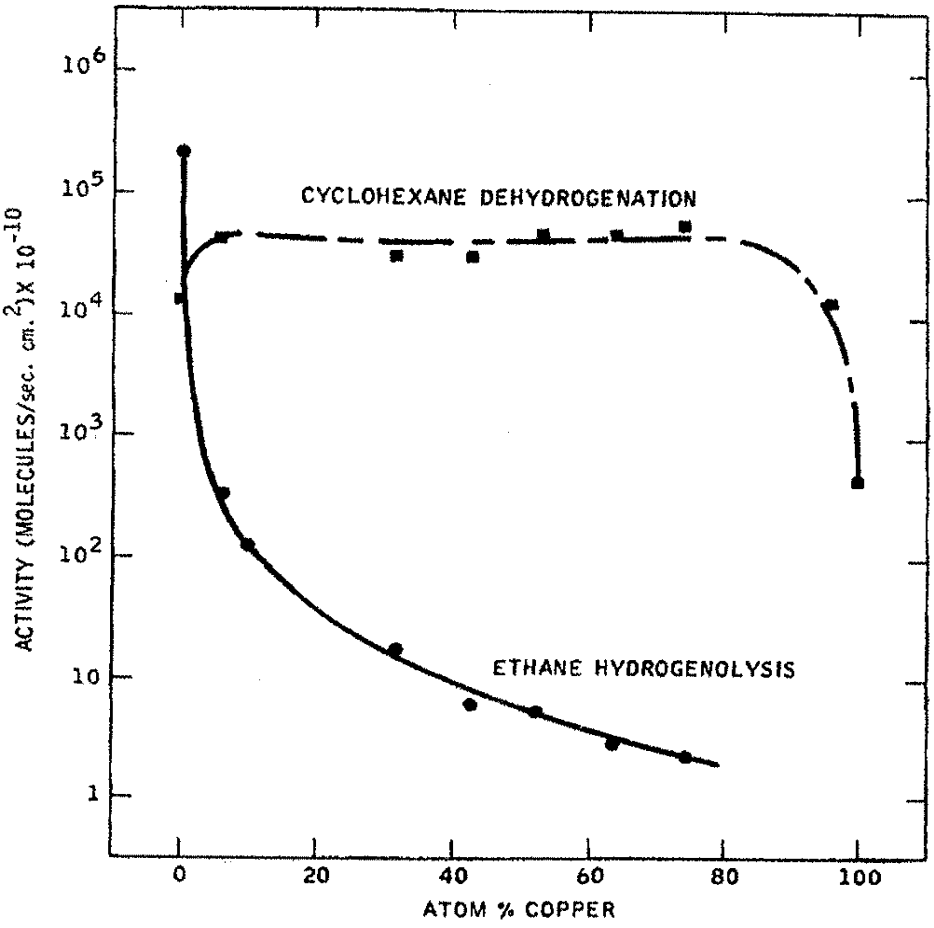

Figure 1. 3 Plot of the activity of bimetallic copper-nickel on cyclohexane dehydrogenation and ethane hydrogenolysis [18]

Figure 1.4 shows the specific activity of the Rh, Ru and Pd towards hydrogenolysis of ethane to methane. One of the most frequently used metals has been cobalt. Cobalt -based catalysts are highly attractive for F-T synthesis. This is due to their high activity, selectivity for linear hydrocarbons, low activity for the competing water-gas shift reaction, and the lower price compared to noble metals [19].

Cobalt based catalysts are widely used in reactions of CO and H_2 as well to form linear aliphatic hydrocarbons. Higher synthesis rates have been achieved by adding ruthenium to the cobalt catalysts [20]. Rh-Co/SiO_2 catalysts showed remarkable methanol formation in CO_2 hydrogenation. The selectivity to methanol increased with the surface composition of rhodium on cobalt. Similarly, palladium has proven to be a useful bimetal with cobalt for hydrogenation reactions. It has been established that palladium facilitates the reduction of cobalt, which can segregate to the catalyst surface. During the catalytic hydrogenation of Co over a catalyst with the ratio of Co/Pd = 2, a synergism was observed, while this was not seen during reactions using individual cobalt and palladium catalysts [42].

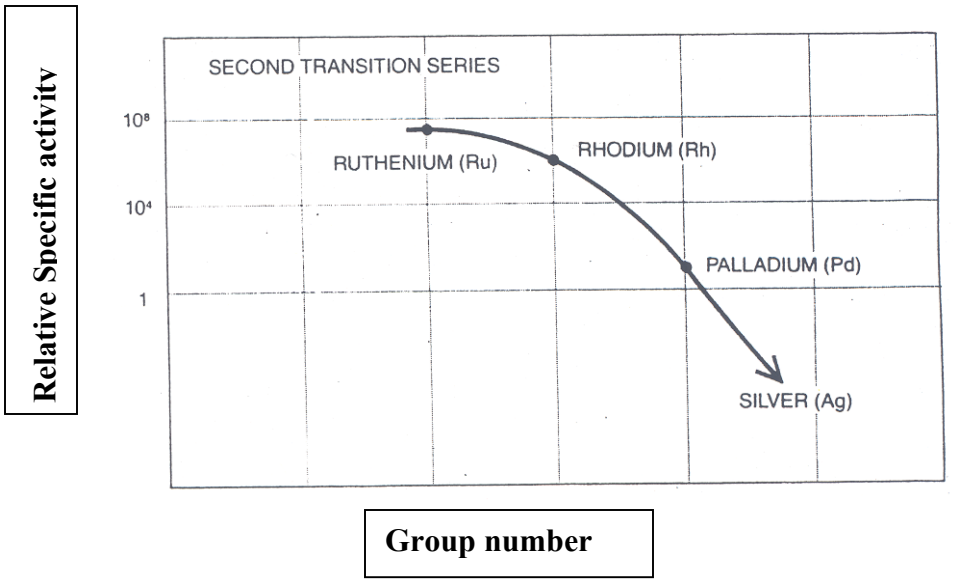

Figure1. 4 Activity of group VIII elements towardshydrogenolysis of ethane to methane [21]

Focus of research

Catalytic hydrogenation of CO_2 has advantages compared with CO_2 deposition and its disposal. It can convert carbon dioxide to other products. As a result, resources of carbon such as natural gas and petroleum will be conserved. The importance of using hydrogen is that it is obtained easily; therefore, methanation of carbon dioxide will be a suitable process for carbon fixation. The real potential of CO_2 utilization requires the consideration of energetic and economic parameters, and careful comparison of the environmental impact of existing and innovative processes [13].

The focus of this research is to study and understand catalyst characterization of bimetallic methanation catalysts. The primary bimetallic catalysts of focus are group VIII elements. The group VIII metals are invariably the most active towards hydrogenation reactions, although their relative activities differ from one reaction to another. The catalyst support used in these studies is silica gel, as it is cheap and readily obtainable.

The objectives of this thesis project are:

To study and characterize bimetallic combinations of rhodium, palladium and ruthenium with cobalt catalyst, which are useful methanation catalysts for carbon dioxide. The project deals with the preparation of these bimetallic catalysts using the co-precipitation and the impregnation methods. These methods are commonly employed for heterogeneous catalyst synthesis. The study focuses on the detection of bimetallic alloys/particles that may be on the catalyst surface, using the surface characterization techniques such as XPS, TPR, SEM and the physisorption methods

.

CHAPTER II

EXPERIMENTAL METHODS

This chapter focuses on the experimental part of the thesis. The first part of it is the catalyst preparation, which explains the basic preparation techniques used in this study. The next section discusses the catalyst characterization techniques used.

Silica support

The support for the catalysts used in this work is SiO_2. The usefulness of silica as a catalyst support comes from its large surface area. This large surface area provides the support for the catalyst metals. This in turn gives great advantage for carrying out reaction studies on silica-supported catalysts. Silica supports are textural promoters and they increase the number of surface sites in the fresh catalyst [22]. Physisorption was used to characterize the silica. The results of the physisorption studies on silica are described in chapter 3.

Bimetallic catalyst preparation

Preparation of catalyst by co-precipitation (General Scheme)

In this method, the precursors of the active components are first dissolved in water or any suitable solvent to form a homogeneous solution. This solution is then subjected to pH adjustment and/or evaporation to precipitate the salts. During this precipitation the salts may be hydrolyzed into hydroxide or oxide forms [23]. This step is referred to as the hydrothermal process. The growth of crystals and their aggregation are influenced by the changes in temperature, the concentration of the salt, the pH, and the rate of pH change. To avoid the introduction of alkali metal in the final catalyst, the pH is often increased by adding ammonia/water. The high concentrations and abrupt changes result in smaller particles and larger aggregation. The solid mass is then dried to approximately the boiling point of the medium. Temperature is gradually increased at a rate of about 2-5^{0}C per min., to allow the water or solvent to evaporate and help the component molecules to attain even redistribution [23].

The dried mixture is now subjected to calcination. During calcination at temperatures of 200-350^{0}C, the precursor salts (here nitrates) are oxidized to form the oxides. The catalyst solidifies into final form; from amorphous to crystalline, hence the mechanical and surface properties are mainly decided in this process. Therefore the heating process must be slow, about 5^{0}C per min., to allow the component molecules to develop a stable structure with fewer strains. Slow evaporation of moisture also results in development of tiny pore channels rather than voids. To ensure the thermal stability of

the catalyst during the reaction, the final temperature is around 50^0C higher than the intended reaction temperature. Reduction in a hydrogen atmosphere is performed to obtain the catalyst in the metal form. The catalyst is now ready for further studies [23]

Preparation of Pd-Co/SiO_2 by co-precipitation

Prior to the preparation, the silica support was degassed on the Autosorb apparatus. The precursors used for preparing this catalyst were cobalt (II) nitrate hexahydrate (99.999%-Co) and a palladium nitrate solution. A complete listing of chemical properties of cobalt nitrate is given in Table 2.1 and Palladium Nitrate in Table 2.2.

2 ml of deionized water was mixed with 0.1452 grams of cobalt nitrate until a uniform colored solution appeared. Then, 0.1171 grams of palladium nitrate was added to this solution. On addition, a dark brown colored solution was formed. After the palladium nitrate was solubilized, 3 ml of deionized water was added. The contents were mixed thoroughly, at which point 0.9311 grams of silica was added. Heating was done at 100^0 C. The pH of the solution was tested and was observed to be 3.4. Approximately 1 ml of ammonium hydroxide (normality 14.8) was added to raise the pH to 8. This was done to precipitate the contents on the support. Uniform stirring with heating continued until all of the contents precipitated on the surface and a chocolate brown mixture was observed.

Drying of the resulting mixture was performed at 120^oC [24]. The sample was dried for 16 hours at this temperature. The observed color of the sample on cooling to room temperature was a brownish yellow color. Calcination of the catalyst was done at 400^oC, starting with a temperature ramp from 100^oC with a ramp rate of approximately

5°C/min. The sample was heated at 400°C for 2 hours. The Pd-Co catalyst in oxide form was obtained. The color was **brownish black** on observation. The preparation scheme is summarized as a flowchart in Figure 2.1.

Table 2.1 **Properties of Cobalt Nitrate**

Chemical Name	Cobalt (II) nitrate hexahydrate (99.999%-Co)
Chemical Family	Metal nitrate salts
Synonym	Cobalt dinitrate hexahydrate, Cobaltous nitrate hexahydrate
Physical and Chemical Properties	
Color and form	Red to purple powder
Molecular weight	182.99
Odor	None
Specific gravity	1.87
Solubility in water	133.8 g/100 cc (0^{o}C)
Stability	Air and moisture stable
Incompatibility	Reducing agents, organic matter, phosphorus and sulfur
Decomposition products	Nitrogen oxides and cobalt salts.

Table 2. 2 Properties of Palladium (II) Nitrate

Trade name	Palladium (II) Nitrate
Chemical Family	Inorganic Salt
Synonyms	Nitric acid, palladium (2+) salt hydrate, palladium dinitrate hydrate.
Physical and Chemical properties	
Color and form	Red-brown crystalline powder.
Odor	None
Solubility in water	Soluble, decomposes
Stability	Stable

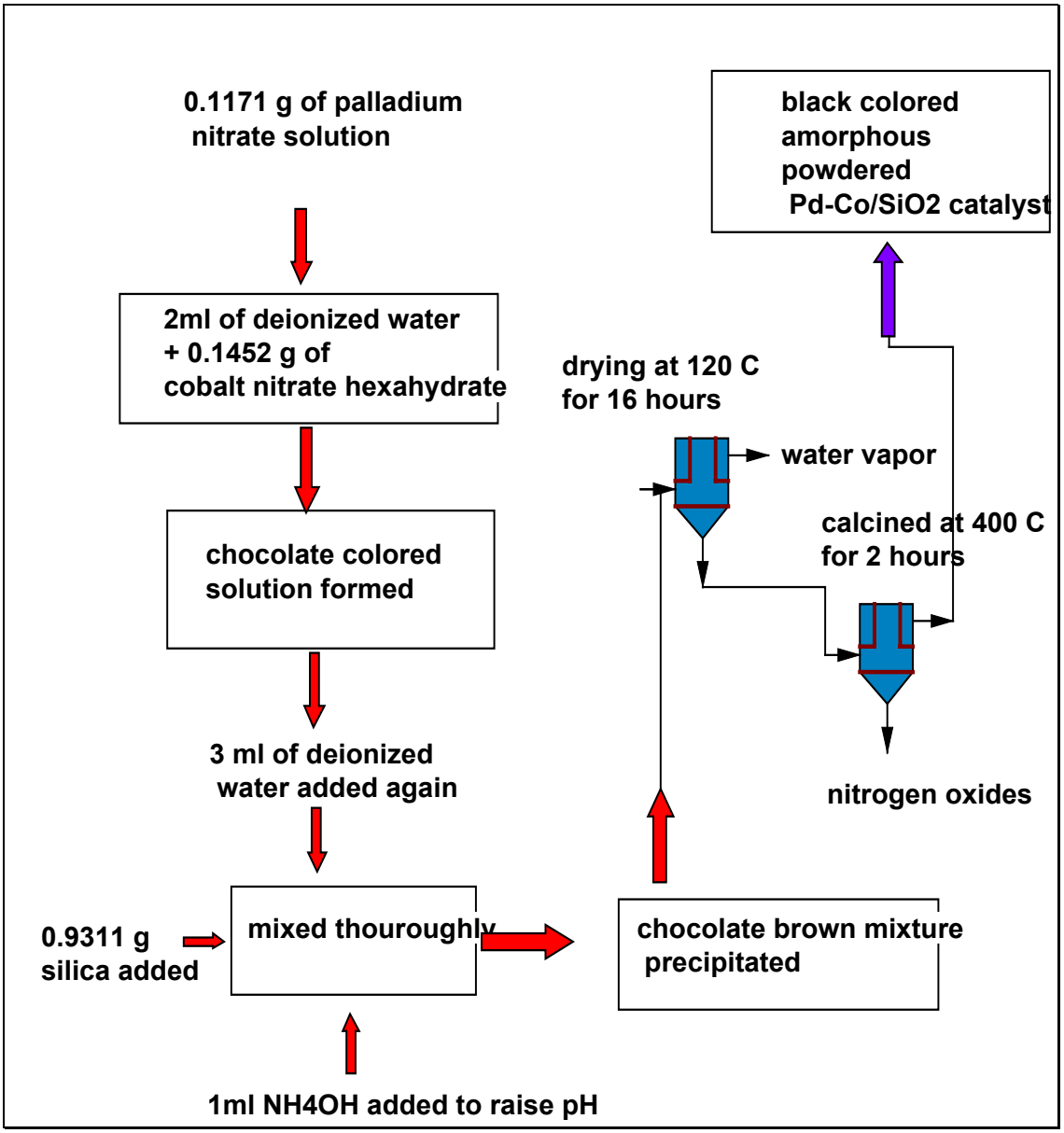

Figure 2.1 Flow chart scheme of Pd-Co/SiO_2 preparation

Preparation of catalyst by Impregnation (General Scheme)

In this method, the catalyst support with desired size and shape, whose pore volume is known, is coated or impregnated on the surface by a solution of the precursor mixture. When the amount of solution added is sufficient to give the required metal content, but not exceeding the pore volume of the support, then the method is known as the Incipient Wetness Technique. As a result, the solid remains a paste. This avoids waste of the active ingredients that can cause an error in the composition.

The method of incipient wetness involves the following steps. First, the support is evacuated, which will give a more uniform distribution of the active component. Evacuation removes trapped air in the pores of the support, which would prevent complete solution penetration, if not removed. Second, the precursors solution is contacted with the support. Third, the excess solution is removed. This is usually carried out by filtration. Fourth, the support is dried. During this process, much of the water is evaporated. Usually a precipitation or a washing step is carried out before or after drying.

Generally, preliminary information regarding the equilibrium distribution of the solution between the solid support and the impregnating solution is required. This information is necessary to obtain the quantity and concentration of the impregnating solution needed to obtain the desired concentration of the active component on the support [25]. If all the salts cannot dissolve at one time, the process may be repeated several times. Upon impregnation of the catalyst to the support, it is then dried, calcined or reduced as described. This method does not produce a high concentration or even dispersion of catalyst components on the surface, but is faster and allows final configuration and properties to be controlled in advance.

Figure 2.2 shows a schematic of the different stages involved during the preparation of impregnated metals on the support.

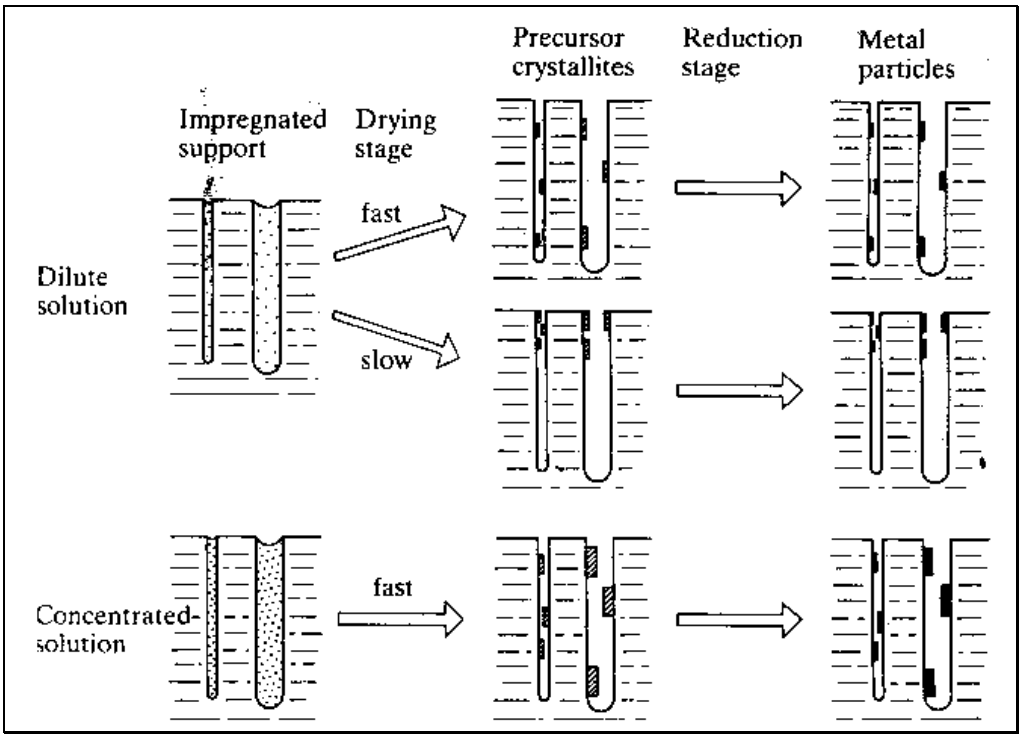

Figure 2. 2 Illustration of the different stages involved during the preparation of supported metal catalysts {Bond et al., 1999}

Preparation of Rh-Co/SiO_2 catalyst by impregnation

Prior to the preparation, the silica support was degassed on the Autosorb apparatus. The precursors used for preparing this catalyst were cobalt (II) nitrate hexahydrate (99.999%-Co) from Strem Chemicals, Inc., and Rhodium (III) nitrate, solution (10% Rh) also from Strem Chemicals, Inc. Detailed information for these chemicals is given in Table 2.1 and 2.3.The metal loading of Rh was at 5 % (by weight) To accomplish this, 0.5067 grams Rh $(NO_3)_3$ solution was measured in a graduated cylinder. Next, 0.1450 grams Co $(NO_3)_2$. $6H_2O$ was added to it, until a red colored solution was formed.

This solution was diluted to 1 ml in the graduated cylinder by adding a few drops of deionized water. Then 0.9220 grams of silica gel was taken in a clean and clear crucible. Drops of the red solution were added intermittently to the silica powder, which was mixed continuously until a **yellowish orange colored powder** was formed. The BET surface area, pore volume, and pore size distribution of the silica gel sample was determined using the Autosorb-1.

The orange yellowish colored catalyst was then placed in a vacuum jar. The jar was then placed in the Lindberg Blue M vacuum oven. The starting set point temperature was the observed room temperature. The ramp rate was 5^0C / min until 200^0C. Then the catalyst was held at a temperature of 200^0C for two hours [16]. The sample was calcined at 300^0C for five hours. The jar was removed after cooling the temperature down to room temperature. The Rh-Co catalyst in oxide form was obtained. A black colored powder was formed. Figure 2.3 shows the schematic of the preparation.

Table 2.3 Properties of Rhodium Nitrate

Chemical Name **Family Name** **Synonym**	Rhodium (III) Nitrate Solution (10% Rh) Metal nitrate salts Nitric acid, rhodium (3+) salt
Physical and Chemical Properties **Color and form** **Molecular weight** **Odor** **Solubility in water**	 Amber liquid 288.60 None Material is a water solution
Stability **Incompatibility** **Decomposition products**	Air and moisture stable Reducing agents, organic matter, phosphorus and sulfur Nitrogen oxides and rhodium salts.

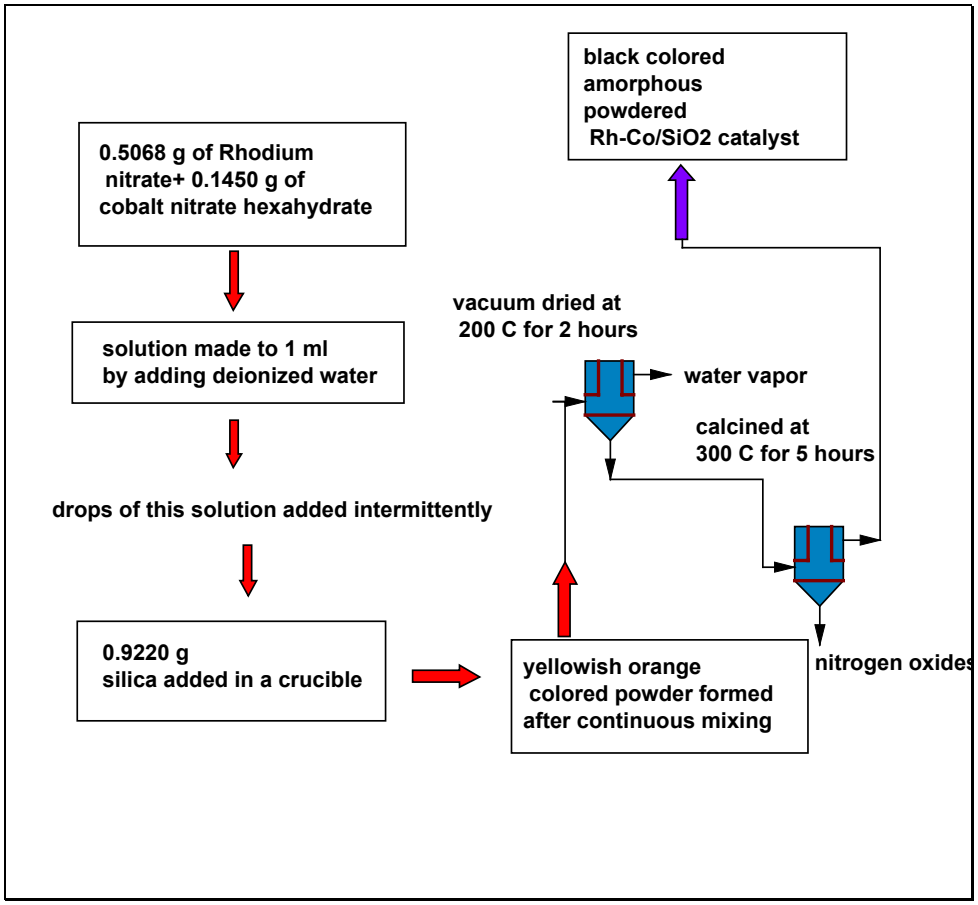

Figure 2. 3 Flowchart scheme of Rh-Co/SiO_2 preparation

Preparation of Ru-Co/SiO_2 catalyst by co-impregnation

Prior to the preparation, the silica support was degassed on the Autosorb apparatus. The precursors used for preparing this catalyst were cobalt (II) nitrate hexahydrate (99.999%-Co) and ruthenium chloride, Detailed information about is provided in Tables 2.1and 2.4

The metal loading of Ru was 5 % by weight. After weighing the required amounts of the precursors, a clean and dry crucible was used. To accomplish this 0.1028 grams of $RuCl_3$ and 0.1435 grams of cobalt nitrate were mixed carefully in the crucible to prepare the catalyst. 1 ml of deionized water was added to the mixture. The mixture was mixed thoroughly until it was uniform in color. A dark black colored solution was formed. Another clean and dry crucible was taken and 0.9214 grams of silica was added. Then drops of this black solution were added intermittently to the silica using a syringe to silica, to prepare the catalyst using the incipient wetness technique. Continuous mixing was done in the process. After all of the solution was mixed with the silica, a light black colored powder was formed.

Ramping to 115^{o}C was done from room temperature at approximately 6^{o}C/min, followed by drying at 115^{o}C for five hours [19]. The substance was cooled to room temperature by slow ramping at 15^{o}C intervals. After drying, the sample was left in the oven at the room temperature for about 36 hours. Next, the sample was calcined at 300^{o}C for two hours with 50^{o}C interval steps starting from room temperature.

Cooling down to room temperature was done with the same ramping intervals. After cooling operations the Ru-Co catalyst in oxide form was obtained. The color of the

sample observed was **black amorphous powder** a detailed preparation scheme is illustrated as a flowchart in Figure 2.4.

Table 2. 4 Properties of Ruthenium Chloride

Trade name	Ruthenium Chloride
Formula	$RuCl_3.3H_2O$
Synonyms	Ruthenium (III) chloride trihydrate, ruthenium trichloride.
Physical and Chemical properties	
Color and form	Red-brown black crystal powder.
Freezing point	20^0C
Boiling Point	Decomposes at 300^0C
Specific Gravity	3.11
Odor	Soluble, decomposes
Solubility	Very soluble
Stability	Stable

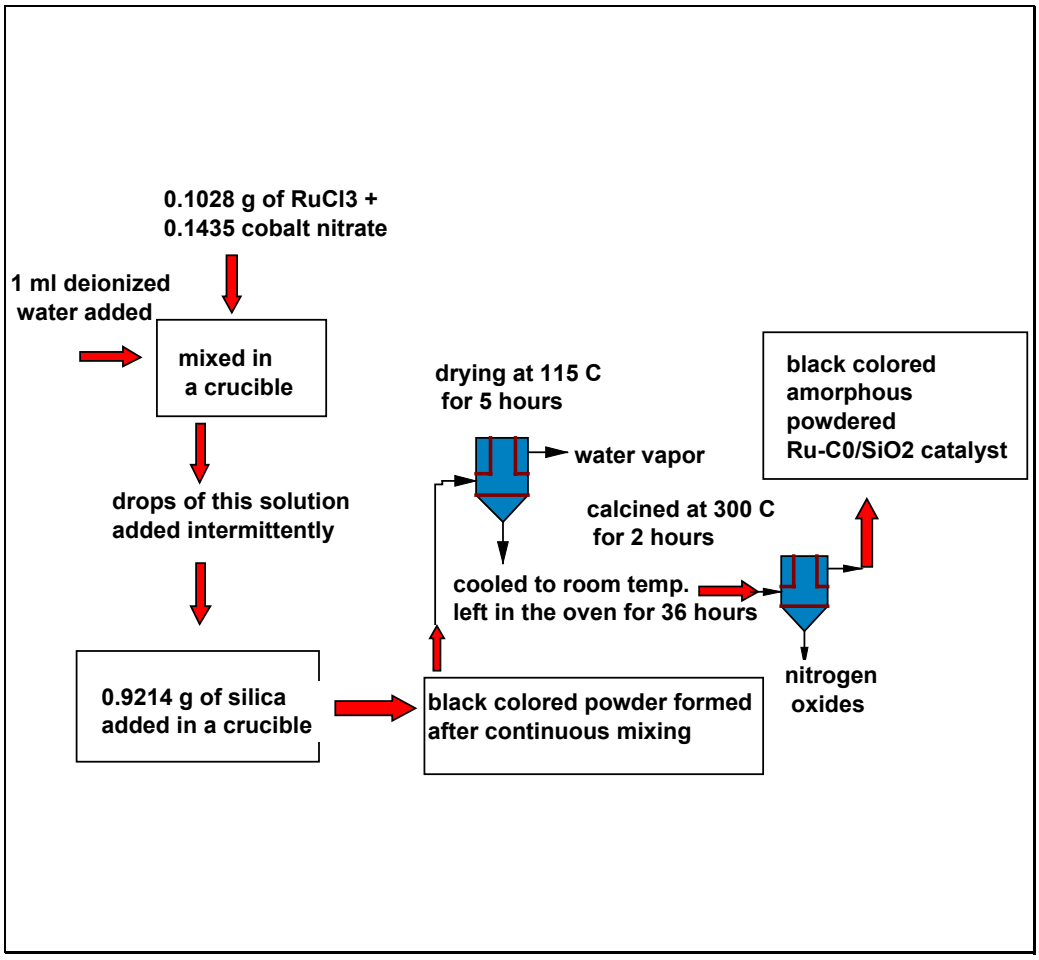

Figure 2.4 Flow chart of Ru-Co/SiO_2 preparation

Physisorption studies

Background

Adsorption is the process where the atoms or molecules of one component become attached to the surface of the other. The former one is termed as the adsorbate and the latter, the adsorbent. In heterogeneous catalysis, the adsorbate and the adsorbent are in two different phases.

Two types of adsorption are physical adsorption and chemical adsorption or chemisorption. Physical adsorption is basically a surface phenomena, and does not involve any chemical reactions. It is reversible and involves small heats of adsorption close to the heats of liquefaction. Physical desorption is essentially nonspecific with respect to the adsorbent and the adsorbate [25]. Physical adsorption, also known as physisorption, has a fundamental significance with respect to heterogeneous catalysis. Physical adsorption studies play a major role in characterizing a catalyst. These adsorption measurements tell more about the extent of the solid surface area and the pore structure of the solid. The determination of the catalyst area has become essential in the reproducible preparation and the systematic comparison of catalysts. Pore structure characteristics like pore volume and pore radius from adsorption data help to establish the reproducibility of catalyst preparation.

Nitrogen Adsorption on Silica

The most common of the adsorbates used is nitrogen. The monolayer region for nitrogen is the region of relative pressure, p/p_0 less than 0.1. The multilayer region for nitrogen is referred to the portion of the isotherm above a relative pressure of 0.1, and the capillary condensation region from 0.4 to 1.0 relative pressure regions.

Brunauer Emmet and Teller Isotherm (BET)

The BET multilayer theory is an extension of the Langmuir's theory of monomolecular surface adsorption. The major assumption used in the BET isotherm is that is that the heat of adsorption for the layers other than the first equals the heat of liquefaction of the bulk adsorption material.

The BET expression is given as

$$\frac{p}{w[(p_0/p)-1]} = \frac{1}{w_m c} + \frac{(c-1)p}{w_m c p_0} \qquad \textbf{(1)}$$

w is the total amount adsorbed at the measured pressure p (mm of Hg)

w_m is the amount adsorbed in the monolayer, (g)

p_0 is the saturation pressure of the adsorbate gas and (mm of Hg)

c is a constant related exponentially to the heat of adsorption and the heat of liquefaction of the adsorbate.

The linearity of equation (1) indicates that a plot of the data within the limits will give a straight line from which the values of the two constants, w_m and c are obtained [26].

Surface area determination from the BET equation using the Multipoint Method

The surface area from the BET theory is determined using equation (1). A plot of $\frac{1}{w(p_0/p-1)}$ versus p/p_0 will yield a straight line, for the data in the range 0.05 $\leq p/p_0 \leq 0.35$.[27]

The slope, s and intercept, i, of a BET plot are:

$$s = \frac{c-1}{w_m c} \quad \textbf{(2)}$$

$$i = \frac{1}{w_m c} \quad \textbf{(3)}$$

Thus from the two equations (2) and (3):

$$w_m = \frac{1}{s+i} \quad \textbf{(4)}$$

and $$c = \frac{s}{i} + 1 \quad \textbf{(5)}$$

Therefore, the total surface area is calculated from equation (6):

$$S_t = \frac{w_m NA}{M} \quad \textbf{(6)}$$

Where S_t is the surface area of the adsorbent in m^2

N is the Avogadro number, (6.022×10^{23} molecules/mole)

A is the area of cross-section of nitrogen molecule = 16.2 Å

M is the molecular weight of nitrogen (g/ mole)

The specific surface area is obtained by dividing this total surface by the sample weight. The c constant for nitrogen lies between 50-250 on most solid surfaces [26].

Total pore volume

The total pore volume is calculated from the amount of vapor adsorbed at a relative pressure of 1. The volume of nitrogen adsorbed (V_{ads}) at the relative pressure is transformed into volume of liquid nitrogen (V_{liq}) by the equation:

$$V_{liq} = \frac{P_a V_{ads} V_m}{RT} \qquad \textbf{(7)}$$

Where: P_a is the ambient pressure, T is the ambient temperature, and V_m is the molar volume of the liquid adsorbate and is equal to 34.7 cm^3 / mol for nitrogen.

X-ray Photoelectron Spectroscopy

X-ray Photoelectron Spectroscopy (XPS) was developed in the mid-1960s by Kai Siegbahn and his research group at the University of Uppsala in Sweden. This technique is also known as ESCA (Electron Spectroscopy for Chemical Analysis). XPS is a very useful technique for characterizing a catalyst material. Identification of the elemental surface composition of the sample and its chemical oxidation state is possible. Surface analysis by XPS is accomplished by irradiating a solid in vacuum with monoenergetic soft x-rays and analyzing the emitted electrons by energy. The survey scan is a plot of the binding energy in eV of the electrons of the elements versus its intensity measured as detected electrons- per -energy interval.

Each element has a unique spectrum. Based on the characteristic spectrum, the element can be identified. Quantification of the peaks observed is done by software. These quantitative data are obtained from the peak areas or the peak heights. The XPS experiment generally employs either AlK_α (1486 eV) or MgK_α (1254 eV) x-radiation [27]. These photons have limited penetrating power in a solid on the order of 1-10 micrometers [28].

Theory

The interaction of photons with the atoms in the surface region causes electrons to be emitted by the photoelectric effect. These emitted electrons have the kinetic energies given by

$$K.E = h\nu - BE - \phi_S \qquad \textbf{(8)}$$

Where BE is the binding energy of the atomic orbital from where the electron originates. hν is the energy of the photon, and ϕ_S is the spectrometer work function. Thus, the binding energy is the difference between the initial and final states after the photoelectron has left the atom. Because each element has a unique set of binding energies, XPS can be used to identify and determine the concentration of the elements on the surface. Variations in the elemental binding energies (chemical shifts) arise from the differences in the chemical potential and polarizability of compounds. These chemical shifts can be used to identify the chemical state of the materials being analyzed [28].

Photoelectron Lines

These lines are the most intense lines observable and are typically the narrowest lines observable in the spectra. Less intense photoelectron lines at higher binding energies are usually wider by 1-4 eV than the lines at lower binding energies.

Energy Loss Lines

For some materials due to the interaction of the photoelectron and the other electrons at the surface, there occurs some loss of energy. This energy loss phenomenon produces a distinct hump, normally 20-25 eV above the binding energy of the parent line, and is known as the energy loss lines.

X-ray satellite lines

Associated with every principle peak, there are satellite lines, or peaks, when using AlK_α or MgK_α radiation. They usually have a small percentage of the intensity of the principal photoelectron line. For example the two satellites of O 1s have ~ 5% and ~3.5 % of the intensity and are located 9.6 eV and 11.5 eV, respectively from the principle binding energy peak [27]. Major problems with these lines arise when they cover the principle peaks of less intense ingredients of a sample.

Auger electron spectroscopy

During the photoelectric process, electrons may be emitted because of relaxation of the excited ions remaining after photoemission. These electrons are known as Auger electrons, and the spectroscopic technique used is known as Auger Electron Spectroscopy. The Auger effect occurs approximately 10^{-14} seconds after the photoelectric effect. This Auger electron has kinetic energy equal to the difference between the energy of the initial ion and the energy of the final ion. Thus, it is independent of the mode of the initial ionization.

Auger Lines:

There are basically four types of Auger lines, namely KLL, LMM, MNN and NOO series. The KLL lines are formed when there is an initial vacancy formed by electron jump in the K level. Then there is the final double vacancy created in the L level. In survey scan studies in this work the O KLL series were observable.

Temperature programmed reduction (TPR)

Temperature programmed reduction is a widely used method for catalyst characterization. One remarkable property of TPR is its high sensitivity. It does not depend on any specific property of the catalyst other than the reducible species under study [29]. During the past recent years, TPR study has been applied to both supported and unsupported catalyst systems. The popularity of this has much to do with the fact that TPR instrumentation is relatively cheap and is highly useful. TPR provides both qualitative as well as quantitative information on metal catalysts. TPR's use is much enhanced by its combination with other experimental techniques like temperature programmed desorption (TPD) and thermogravimetry [30].

Thermodynamics

The standard free energy change (ΔG^0) is a function of the temperature for the process reaction.

$$M_n O_m + H_2 \rightarrow M + H_2O \quad \textbf{(9)}$$

For the reaction: $M_n O_m (s) + (m/2) H_2 \rightarrow n M(s) + mH_2O (g)$

ΔG^0 is given in Figure 2.5, which shows that ΔG^0 is negative for a number of oxides, thereby signifying thermodynamic feasibility. However, reduction profiles for vanadium, tin, calcium even though ΔG^0 is positive for each of these reactions.

This is possible because:

$$\Delta G = \Delta G^0 + RT \ln (P_{H20} / P_{H2}) \quad \textbf{(10)}$$

The TPR method is such that all the water formed is driven off from the reaction zone. Thus, when the P_{H2O} is lowered sufficiently, it is possible for the term RT ln (P_{H2O}/P_{H2}) to be negative, thereby nullifying the positive effect of ΔG^0. Thus, the ΔG is lowered, and the reduction profiles can be observed [31].

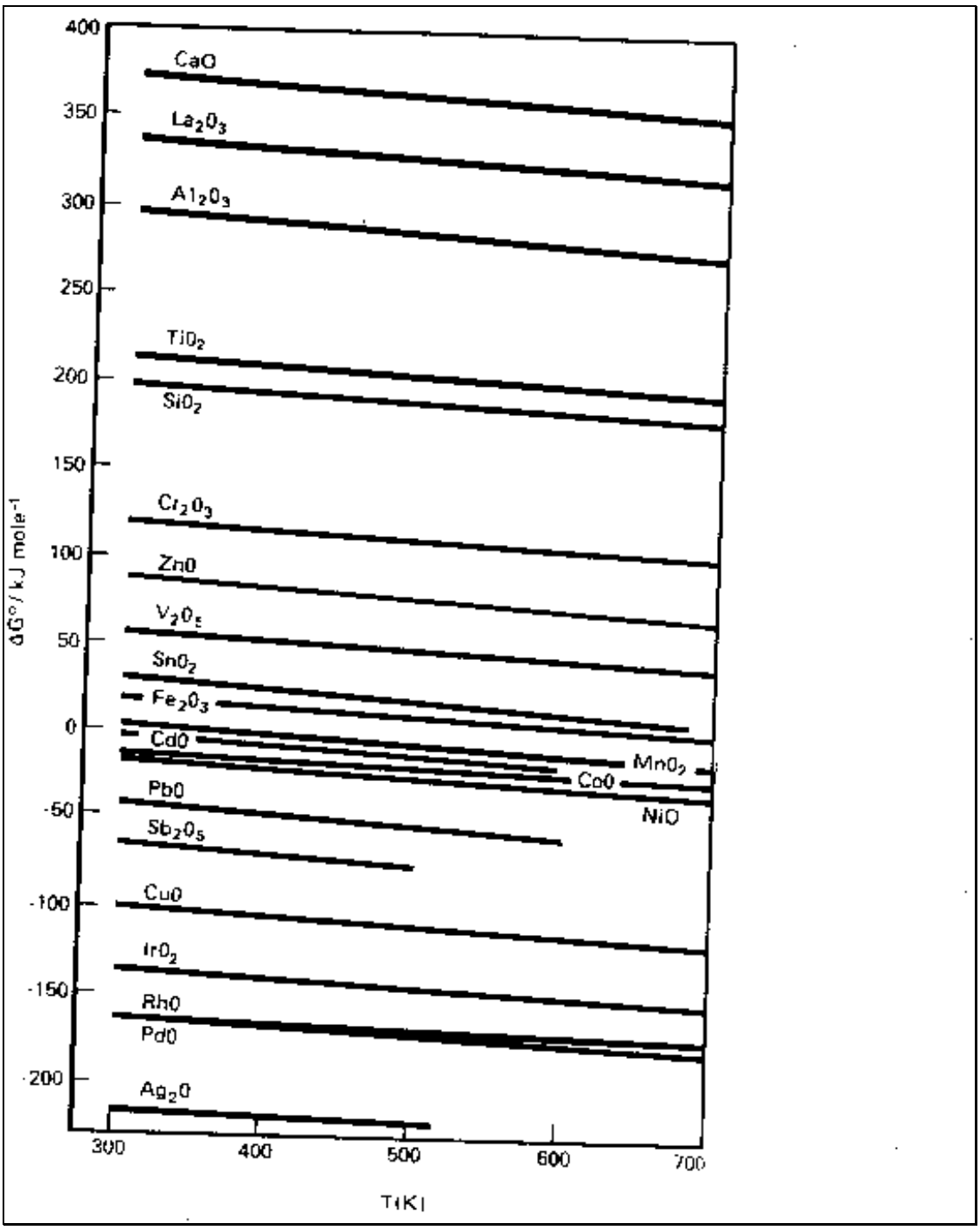

Figure 2.5 Illustrating the standard free energy change (ΔG0) versus temperature [31]

Kinetics and Mechanism

The reduction kinetics that is observed is of the same general form for both supported as well as unsupported (bulk) oxides. Consider the process where a sphere of a metal oxide is reduced to the metal by a flowing stream of Hydrogen. The degree of reduction, α, as a time (t) dependent function, for various temperatures and pressures of hydrogen is a commonly observed factor. All these data constitute the kinetics of TPR and are interpreted in terms of the mechanism by which the reduction occurs. In general, a nucleation model is used to interpret these data

Theory

Temperature programmed reduction determines the number of reducible species present in the catalyst. It also indicates the temperature at which the reduction takes place. The phase of the supported precursor and its interaction with the support can be identified. The TPR analysis usually begins by flowing analysis gas (here we use 5 % hydrogen in an inert carrier gas argon) over the sample. The composition of the gas flowing over the sample is monitored during a linear temperature change.

The sample is the catalyst precursor (oxide state) and the catalyst is the material obtained after reduction. A thermal conductivity detector usually determines the change in the composition of the gas. This detector records the different thermal conductivity of the gas that results due to the changes in the composition. A detailed schematic of the TPR is shown in Figures 2.6 and 2.7.

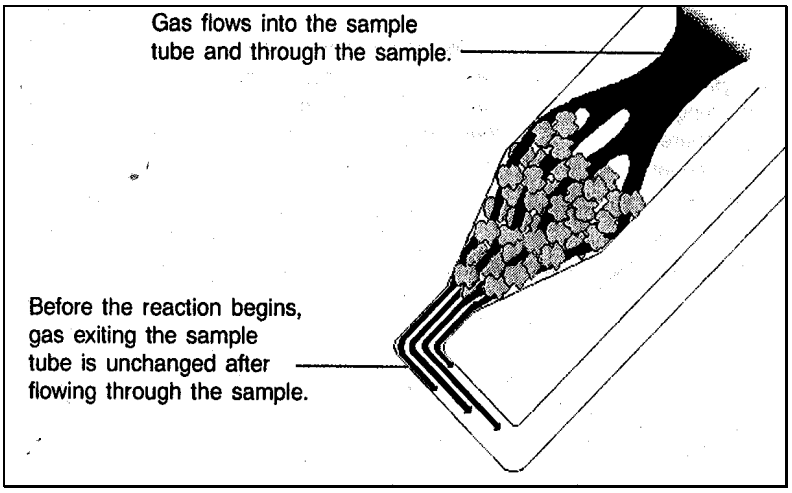

Figure 2.6 Schematic of TPR – 1 [29]

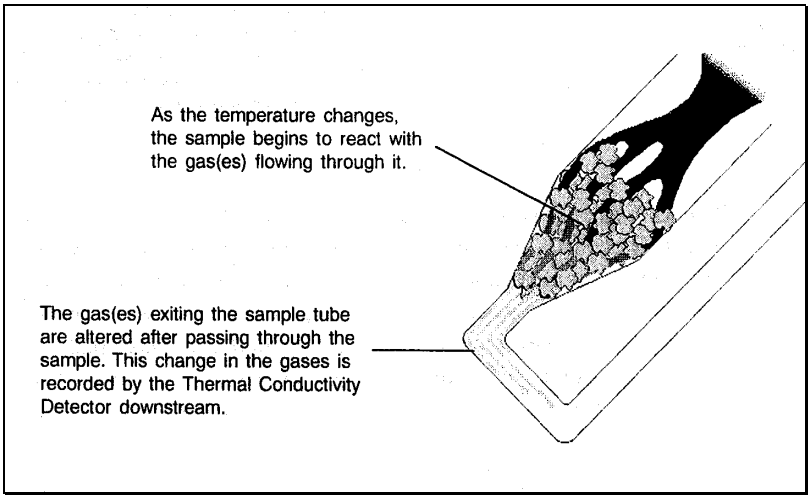

Figure 2.7 Schematic of TPR-2 [29]

The plot of the TPR is a trace of the thermal conductivity versus the temperature of the reaction. The peak position is determined by the environment of the reducible component and by its chemical nature. The peak area reflects the amount of hydrogen consumed in the reaction. TPR is usually carried out at low partial pressures of the reactive gas. Thus, it is possible to observe the intermediate reactions depending on the temperature rate, concentration of reacting gas, and the flow rate. In the case of bimetallic systems, evidence of the interaction between the two metal components is obtained through the TPR studies. The plots produced are characteristic of a particular solid. Based on the peaks obtained at different reduction temperatures, it is possible to determine whether the metals are weakly bound or strongly bound in their molecular/ atomic state.

Electron Microscopy Studies

Electron microscopy is a powerful tool for studying the surface structure of the catalyst sample, preferably with a high-resolution image. These surfaces, which are difficult to perceive with the naked eye, are more clearly observed with magnification, that extends to as high as 100000 X using modern electron microscopes. Two common microscopy studies that are involved with materials characterization are Scanning Electron Microscopy (SEM) and Transmission Electron Microscopy (TEM). In this study only SEM is used.

Scanning Electron Microscopy (SEM) and Energy Dispersive X-ray Spectrometry (EDS)

SEM is one of the widely used and versatile of modern scientific tools, since it studies the morphology and composition of biological and physical materials down to a few nanometers. SEM is usually carried out by scanm ,ning an electron probe over the specimen. Thus, the morphology as well as the topography study of the specimen can be obtained through high or low-resolution images with a great depth of field. Monitoring the secondary x-rays that are produced by the electron interactions also gives composition information on the sample.

How it works?

An X-ray beam strikes the surface of the sample, and as a result of this, the electrons are ejected from or bounced off of these surfaces. These electrons are made to

form an image, which is seen on the computer, or else viewed as a digital image for later computer analysis.

Secondary electrons are electrons emitted from atoms on the surface of the sample and these form the readily obtainable image and are more important in this study. The average energy of secondary electrons is about 3 eV to 5 eV. The standard image in the SEM is mainly composed of these secondary electrons. In general, about 1 percent of the secondary electrons escapes from the surface and contribute to the image formation. The maximum escape depth is about 5 nm in metals [32].

Backscattered electrons are electrons from atoms inside the sample, and the images formed have lower resolution compared to those formed by the secondary electrons. The resolution for an SEM with the backscattered electrons is about 15 nm while that for the secondary electron image is about 4 nm [32]. The image resolution is an important factor in SEM studies. Larger magnification of the image with better resolution helps in focusing the study to greater field depths and these are particularly important in these studies where adsorption of metals on another surface is the issue. The power of the X- ray beam determines the resolution of the image. Thus, better resolution is obtained through the use of a high-energy beam with lower magnification and vice versa. The depth of analysis is also important in studies where elemental composition studies are performed. These elemental analyses are done using the Energy Dispersive X-ray Spectrometry (EDS).

EDS is a useful material characterization technique, as it determines both quantitatively and qualitatively the elemental composition of the specimen sample. SEM-EDS is often used in the surface studies of both biological as well as inorganic samples.

When the beam of the x-ray strikes the sample, shell transitions take place in the atom and as a result, x-rays are produced. These emitted rays, which are characteristic of the energy of the parent electron, are collected and plotted as a spectrum by the computer, which maps the corresponding energy intensity of the x-rays, and thus, identifies the element present. Thus chemical analysis up to a relative error of 1-2 % from larger areas of the solid (0.5-3 micrometer diameter) is possible [33].

CHAPTER III

RESULTS AND DISCUSSION

XPS Results

Results of Ru-Co/SiO_2

XPS analysis for the Ru-Co/SiO_2 catalyst was carried out using a PHI 1600 XPS System. The instrument was calibrated, and the spectrometer work function determined assuming the binding energy of the Au $4f_{7/2}$ peak to be 84.0 eV. AlK_α and MgK_α characteristic X-ray lines with 100 eV pass energy were applied to measure the cobalt and ruthenium spectra. The high-resolution spectrum was taken of the adventitious carbon on the surface of the sample to use as a reference for charge correction. The generally accepted binding energy for adventitious carbon is 284.8 eV. Table 3.1 shows the different surface concentrations of Ru, Co, Si, O, C and N. The angle of incidence was initially set at 45^o.

Figure 3.1 shows the survey scan using AlK_α radiation. No peaks were observed for Ru. A significant amount of surface oxygen (79.1%) was observed. Oxygen and carbon was only present.

Table 3. 1 Surface Concentration in % of un-reduced Ru-Co/SiO_2catalyst, analyzed by XPS

Figure	O 1s	C 1s	Si 2p	Ru 3p	Co 2p3	N 1s	Angle of incidence	Radiation
Ru-Co	79.1	20.9	0	0	0	0	45	AlK_α
Ru-Co	67.4	17.5	14.9	0.2	0	0	45	MgK_α
Ru-Co*	61.8	4.3	32.9	0.7	0.3	0	45	AlK_α
Ru-Co+	44.1	20.0	30.0	0.4	0	5.5	45	AlK_α
Ru-Co	51.6	19.2	28.8	0.4	0	0	90	AlK_α
Ru-Co	51.2	21.1	27.3	0.4	0	0	15	AlK_α

* Measured at different point of incidence compared to the first data point

+ After Ar^+ sputter for 15 min

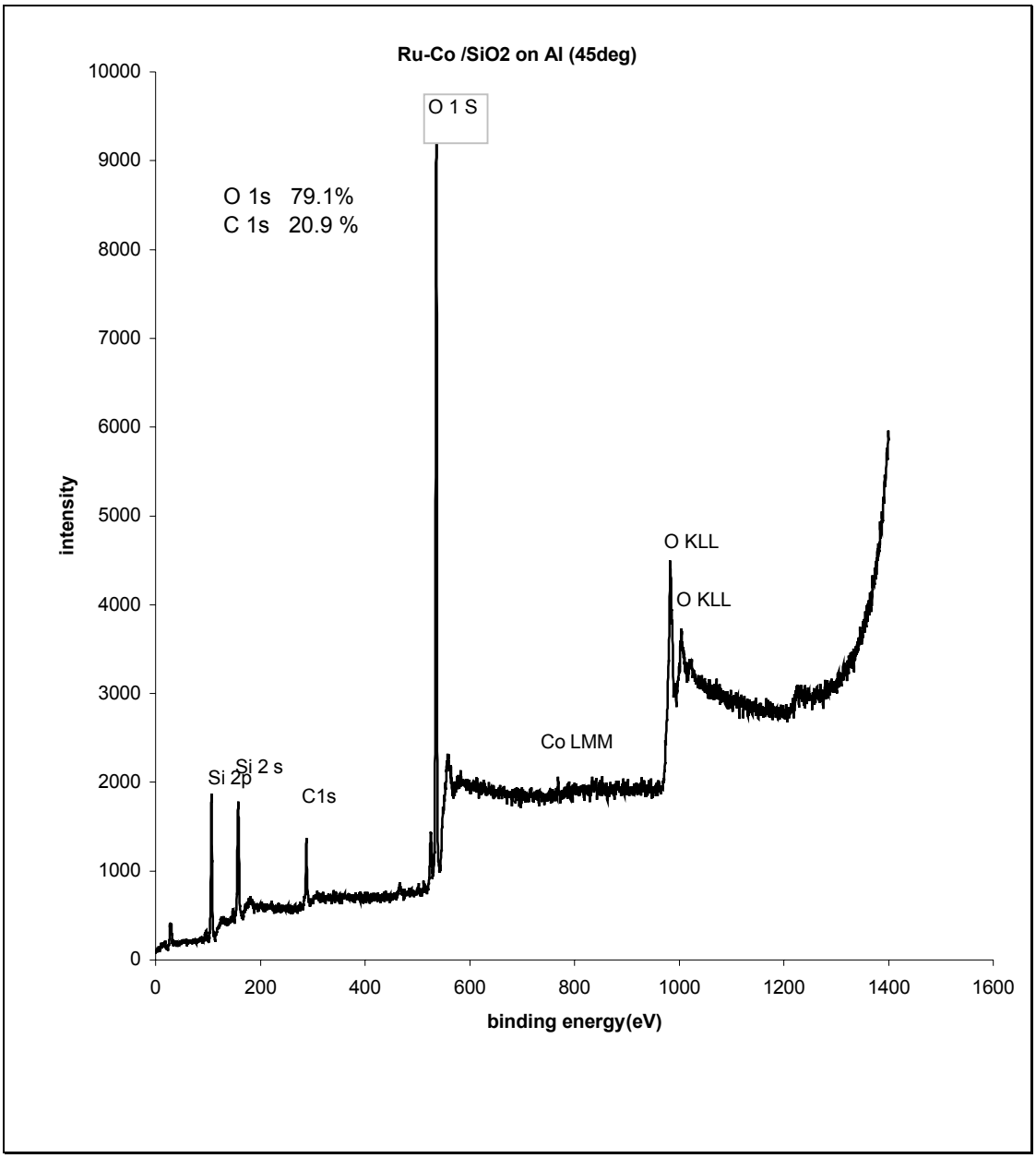

Figure 3. 1 Survey scans of Ru-Co/SiO_2 using AlKα radiation

Figure 3.2 shows the survey scan using MgK_{α} radiation. The oxygen Auger peak is overlapping the Co 2p binding energy region. A peak due to ruthenium at a binding energy of 463.3 eV was observed. Additionally, the O 1s Auger line is known to appear at similar binding energy as Ru 3p. For Ru bimetallic catalyst, the Ru 3d peak was the more intense peak observed, but here it was overlapped by the C1s peak, thus the Ru 3p peak was used. The surface concentration of C 1s remained more or less the same at about 17.5%. The Auger lines for oxygen seen in Figure 3-1, appeared at a different position as compared to Figure 3-2. This is because the Auger lines have kinetic energies, which are independent of the ionizing radiation.

Different point of Incidence effect

Figure 3.3 shows the survey scan by aluminum radiation using a different incidence point. A Ru 3d peak was observed at 281.2 eV which overlaps with the C1s peak. Hence Ru 3p peak was used. Since large quantities of oxygen were present, the intensity data for Ru 3p peak was corrected for oxygen. A change in the angle of incidence should allow the observation of the near-surface region. A peak at 780.3 eV due to cobalt gave a surface composition of 0.3%. The Ru signal increased to 0.7%. A comparison of Figures 3.1 and 3.3 indicate that the distribution of Ru and Co species on the SiO_2 surface was not even. Thus, using a different point of incidence showed Co species initially not observed on Figure 3.1. Another observation was the decrease in the C 1s surface concentration. The increase in the Si concentration offset this result. The

high values of O and C suggested that Ar^+ sputtering was performed to remove surface carbon in the sample. No other elements were detected.

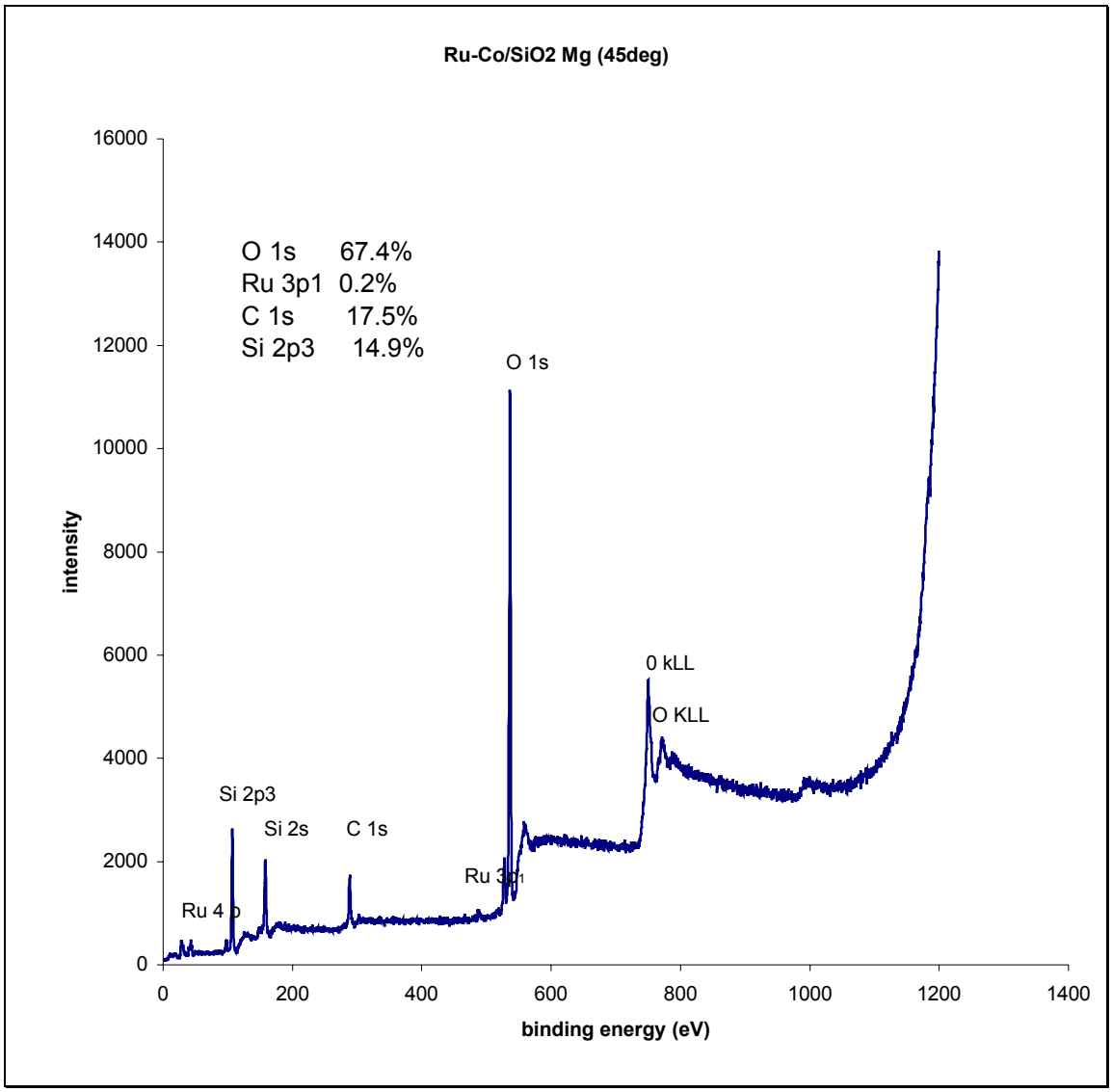

Figure 3. 2 Survey scan of Ru-Co/SiO_2 using MgK radiation

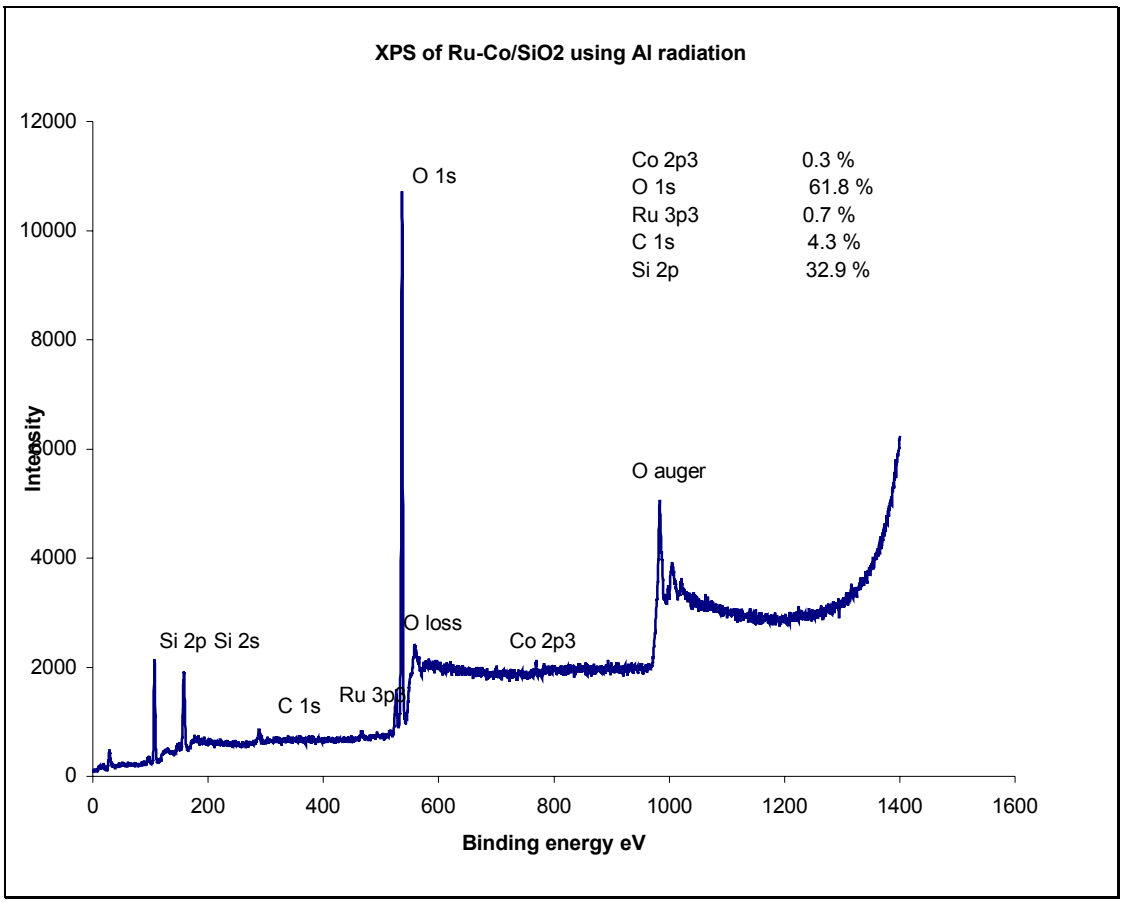

Figure 3. 3 Survey scans spectra of Ru-Co/SiO_2 taken at a different point

Effect of Ar^+ Sputtering

Figure 3.4 shows an XPS spectrum of the catalyst sample after Ar^+ sputtering for 15 min and at a 45^o angle. Notable changes observed include the decrease of the signal due to oxygen to 44.1%, and the appearance of N 1s and an increase in the C composition from 4.3% to 20.0%.

Angle of grazing effect

On the comparison of Figure 3.5 (where the angle was 90^o) and Figure 3-6 (grazing angle 15^o), large differences are not observed in any of the surface composition values. Table 3-2 shows the binding energy values of elemental components of Ru-Co/SiO_2.

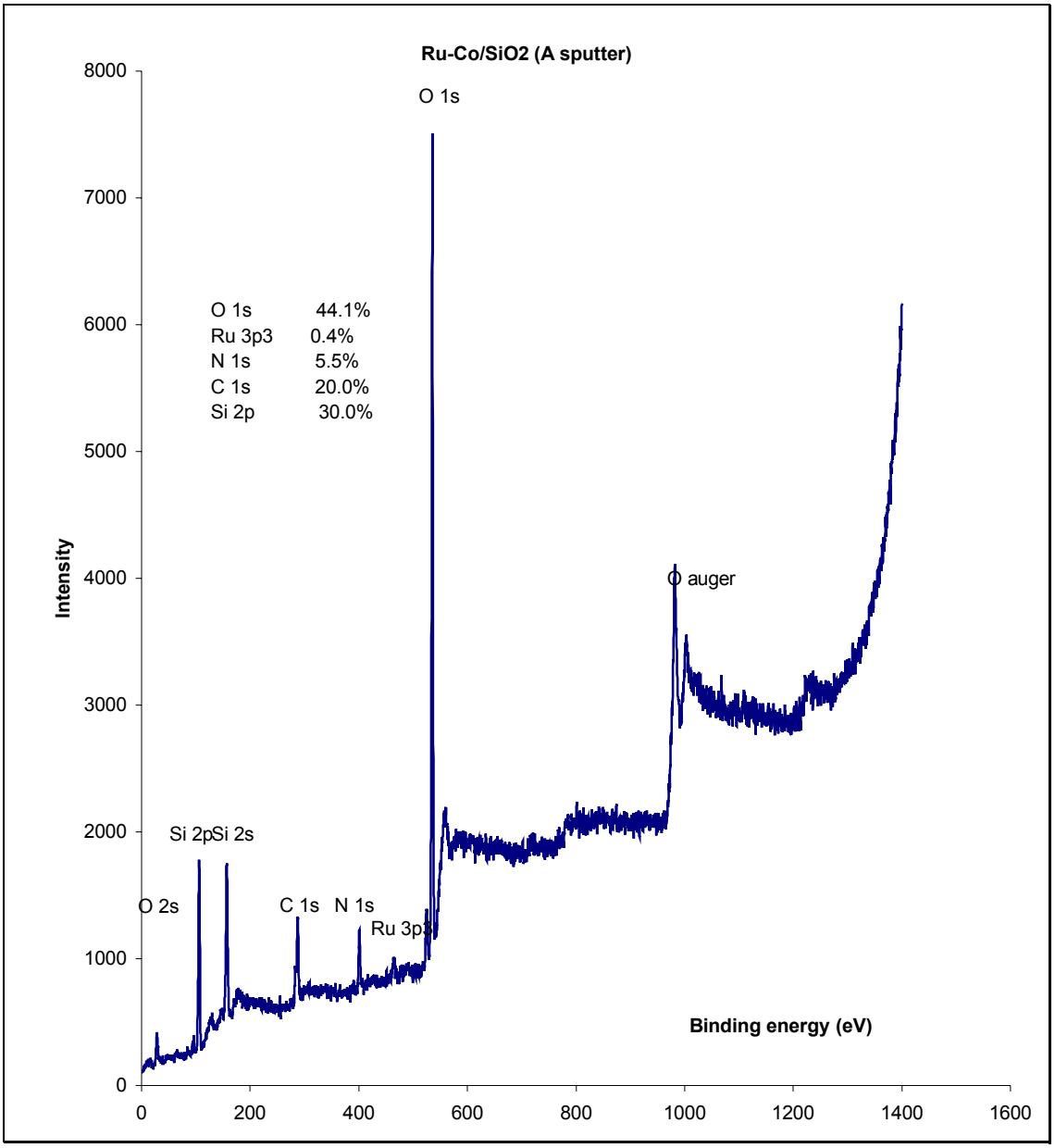

Figure 3. 4 Survey scan spectra of Ru-Co/SiO_2 after Ar^+ sputtering

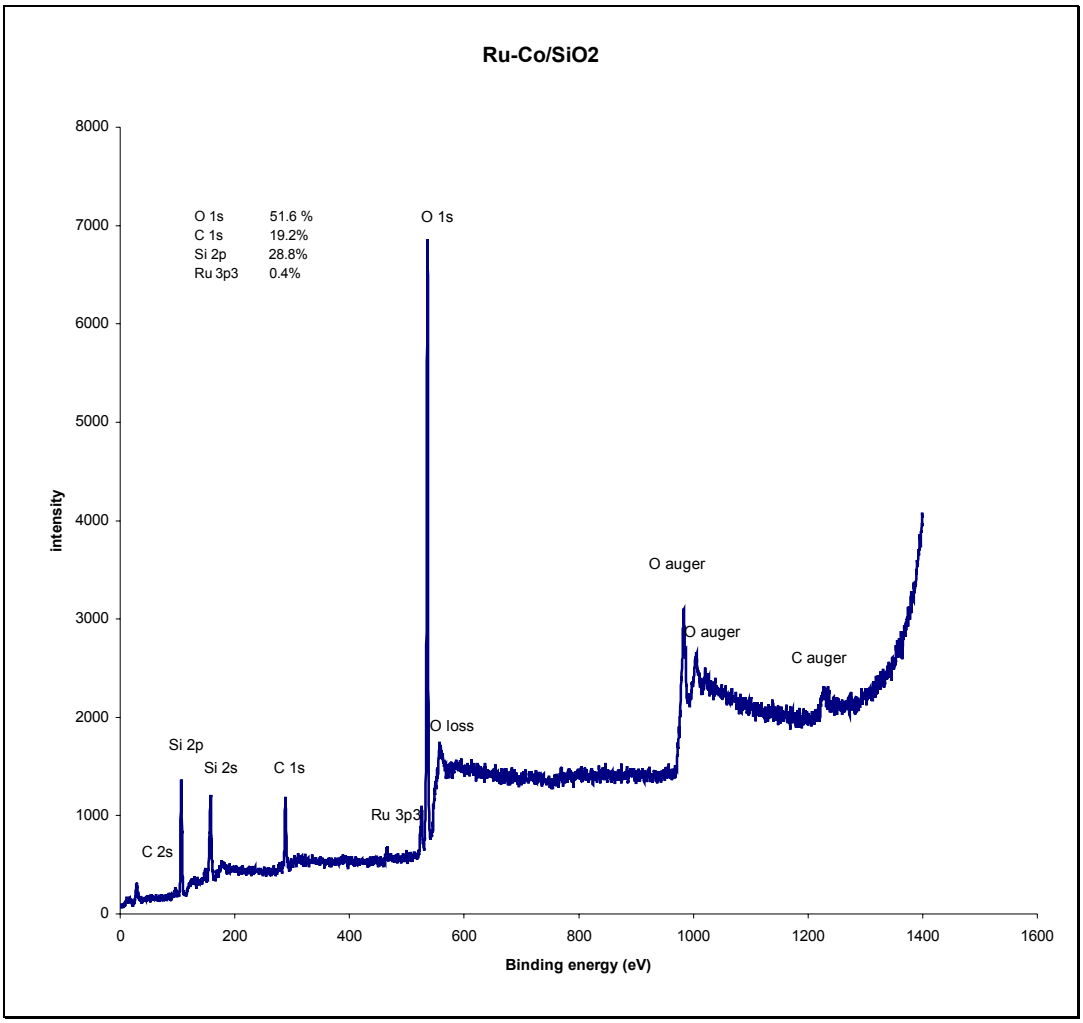

Figure 3. 5 Survey scan spectra of Ru-Co/SiO_2 at 90 degrees grazing angle

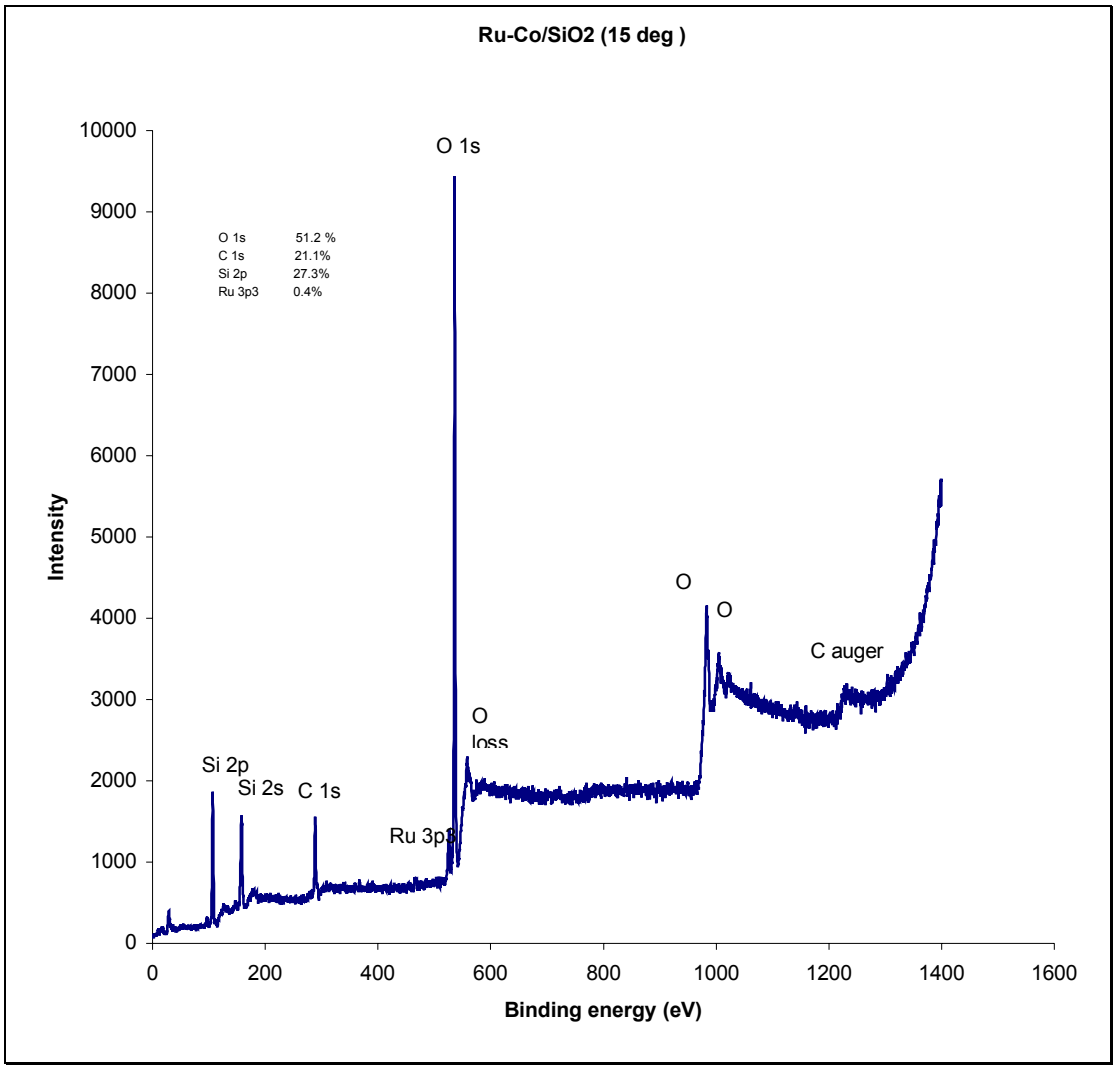

Figure 3. 6 Survey scan spectra of Ru-Co/SiO_2 at 15 degree grazing angle

Table 3.2 Binding energy values in eV of elements of Ru-Co/SiO_2

Figure	O 1s	C 1s	Si 2p3	Co 2p3	Ru 3p3	N 1s
Ru-Co	536.95	288.95	107.45	------	------	------
Ru-Co	537.95	290.45	108.95	------	490.45	------
Ru-Co*	528.7	281.2~ Ru 3d peak	99.2	761.8	458.7	------
Ru-Co+	538.6	290.1	109.1	------	469.1	404.1
Ru-Co	539.9	292.4	110.9	------	469.9	------
Ru-Co	540.9	293.4	111.9	------	468.4	-------

* Measured at different point of incidence compared to the first data

+ After Ar^+ sputter for 15 min

Table 3.3 XPS results of Ru-Co/SiO_2

Sample	Composition	$(Co/Ru)_{bulk}$	Co2p, BE in eV	Ru3p, BE in eV	Co/Si	Ru/Si	$(Co/Ru)_{surface}$
Ru-Co/SiO_2	Ru50Co50	1.00	761.8	458.7	0.009	0.021	0.428

Discussion of XPS results of Ru-Co/SiO_2

The surface compositions for each of the metals Ru and Co were significantly low when analyzed using XPS. Thus, the presence of the metals on the surface was very negligible, and it can be concluded from these experiments that the surface was composed largely of support silica. The change in the grazing angle did not significantly change the surface concentrations of the elements. At 90^0 with respect to the surface plane, the signal from the bulk is maximized relative to that from the surface layer. At small angles the signal from the surface becomes greatly enhanced, relative to that from the bulk.

Comparison of bulk and surface ratios of bimetals

Table 3.3 shows the ratios of Co/Ru in the bulk and at the surface. The Co/Ru ratio at the surface is less compared to those in the bulk. On comparison of Co/Si and Ru/Si ratios at the surface, more Ru is at the surface. Consequently, the comparison of Co/Ru in the bulk and Co/Ru at the surface shows that cobalt species remain in the bulk of the catalyst. Hence, surface segregation of cobalt is observed here.

Alloys/Bimetal Formation

The formation of alloys is most often observed when the catalyst is subjected to oxidative and reductive treatments, and through comparison of the resulting binding energies of the ruthenium and cobalt peaks. If the peak positions change, then one can postulate segregation of these particles. The binding energy of 458.7 eV for the Ru peak is attributed to that of RuO_2. The binding energy for the Co 2p at 761.8 eV is difficult to

interpret and neither can be attributed to any of cobalt alloys referenced in the National Institute of Standards and Technology database. Thus, the XPS results are not definitive in showing alloy or bimetal formation. The TPR analysis should provide more definitive results on alloy formation.

Oxidation state of elements

The Ru 3d and the C1s lines overlap [34] for the XPS of Ru-Co/SiO_2, which are consistent with those of the compounds of CoO and RuO_2. But the Co 2p at 761.8 eV in Ru-Co/SiO_2 catalyst does not clearly indicate the oxidation state of Co. However, based on the presence of RuO_2, it is likely that cobalt also exists in the oxide state. The most likely form of cobalt oxide is CoO. The Ru 3d peak at 281.2 eV suggests that Ru is in +2 oxidation state in the Ru-Co/SiO_2 sample from the reference from National Institute of Standards and Technology website [35]. The value of Si 2p of 107.5 eV for Ru-Co catalyst suggests the presence of SiO_2 at the surface [36]. The Si 2p peak appears at different binding energy values for the samples Ru-Co/SiO_2 for each of the observations. Table 3.8 gives the oxidation state of the elements analyzed by XPS.

Results of Rh-Co/SiO_2

XPS analysis for the Ru-Co/SiO_2 catalyst was carried out using a PHI 1600 XPS System. The instrument was calibrated, and the spectrometer work function determined assuming the binding energy of the Au $4f_{7/2}$ peak to be 84.0 eV. AlK_α and MgK_α characteristic X-ray lines with 100 eV pass energy were applied to measure the cobalt and rhodium spectra. The high-resolution spectrum was taken of the adventitious carbon on the surface of the sample to use as a reference for charge correction. The generally accepted binding energy for adventitious carbon is 284.8 eV. The survey scan in Figure 3.7 revealed large quantities of O and Si as expected. The carbon content was comparatively low at 12.2 %. Table 3.4 shows the comparison of the bulk to surface composition of the elements. Rh and Co composition are expected to be low, due to its lower bulk composition. The fact that this sample was not reduced in H_2 accounts for the larger oxygen content. Ar^+ sputtering was not done on this sample. The absence of nitrogen confirms total oxidation of the cobalt nitrate precursor to its oxide form during calcinations. The Si percentage was very high as expected. This is also attributed to its greater bulk loading during preparation. The charge compensation for the elements is approximately 6.2 eV. No other elements were detected. Table 3.5 shows the binding energy values for the elements.

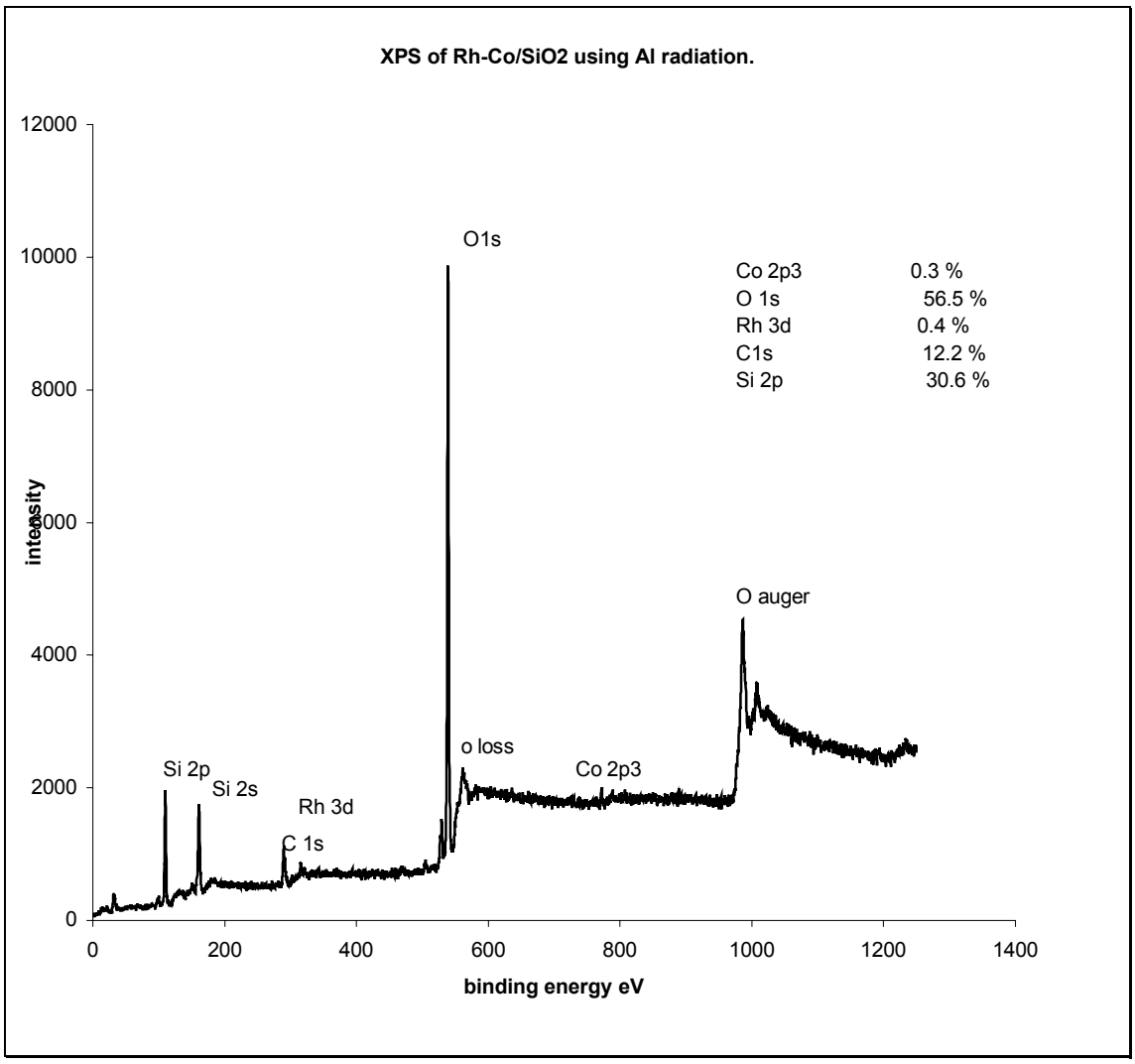

Figure 3. 7 XPS spectrum of Rh-Co/SiO_2 catalyst using Al radiation

Table 3.4 XPS results of Rh-Co/SiO_2

Sample	Composition	$(Co/Rh)_{bulk}$	Co 2p, BE in eV	Rh 3d, Be in eV	Co/Si	Rh/Si	$(Co/Rh)_{surface}$
Rh-Co/SiO_2	Rh50Co50	1.00	778.7	321.7	0.009	0.013	0.75

Table 3.5 Binding Energy (eV) and surface atomic composition values of Rh-Co/SiO_2

Element	**O 1s**	**C 1s**	**Co 2p3**	**Rh 3d**	**Si 2p**
Corrected BE (eV)	545.2	296.2	778.7	321.7	116.2
Experimental BE (eV)	545.2	290	772.5	315.5	116.2
Surface Atomic %	56.5	12.2	0.3	0.4	30.6

Discussion of XPS results of Rh-Co/SiO_2

The surface compositions of Pd and Co were low when analyzed using XPS. Thus, the presence of the metals on the surface is very negligible, and it can be concluded that the surface is composed largely of support silica. This is illustrated in Table 3.4, where the ratio of Co/Rh at the surface is less compared to that in the bulk. On comparison of Co/Si and Rh/Si ratios at the surface, Rh is greater at the surface. Consequently, the comparison of Co/Rh in the bulk and Co/Rh at the surface shows that the cobalt species remain more in the bulk of the catalyst. Hence, surface segregation of cobalt is observed here.

Alloys, Bimetal, Cluster Formation

Nothing particular can be said about the formation of bimetals or alloys based on the core peaks of rhodium and cobalt. No information about XPS Rh-Co alloys was found in the National Institute of Standards and Technology database. TPR results should be a better indication of the alloys formation.

Oxidation state of elements

The Co 2p binding energy at 778.7 eV in Rh-Co catalyst suggests the presence of CoO at the surface [37]. Thus, the Co is in the +1 oxidation state [38] in the Rh-Co/SiO_2 sample. Based on all of the other results, it can be stated that all the metals are likely to exist on the surface as oxides. Thus Rhodium would also be present at the surface as its oxide. Blix et al. [43] reports Rh_2O_3 reduction through TPR results. NIST database lists the Rh 3d binding energy at 303 eV and is different from Rh 3d peak at 321.7 eV in this

work. Therefore, the oxidation state of rhodium is not observable based on XPS results. Table 3.8 gives the oxidation state of the elements analyzed by XPS.

Results of Pd-Co/SiO_2

XPS analysis for the Ru-Co/SiO_2 catalyst was carried out using a PHI 1600 XPS System. The instrument was calibrated, and the spectrometer work function determined assuming the binding energy of the Au $4f_{7/2}$ peak to be 84.0 eV. AlK_α and MgK_α characteristic X-ray lines with 100 eV pass energy were applied to measure the cobalt and palladium spectra. The high-resolution spectrum was taken of the adventitious carbon on the surface of the sample to use as a reference for charge correction. The generally accepted binding energy for adventitious carbon is 284.8 eV. Oxygen and silicon surface concentrations were high, as expected and shown in Figure 3.8. The high silica loading during the catalyst preparation gives the larger Si value. The presence of a large oxygen signal is again due to SiO_2 on the support. The cobalt percentage was negligible. One of the possible reasons would be the migration of the cobalt species from the surface to the bulk or else the oxygen species diffusing from the bulk to the surface of the sample. Ar^+ ion sputtering was done for 15 min. The results showed the presence of nitrogen at the surface with a composition of 5.0%. Table 3.7 shows the surface to bulk comparison of Pd, Co and Si. Table 3.6 shows the binding energy values and the elemental composition of the elements. The charge compensation was 3.1 eV. No other elements were detected.

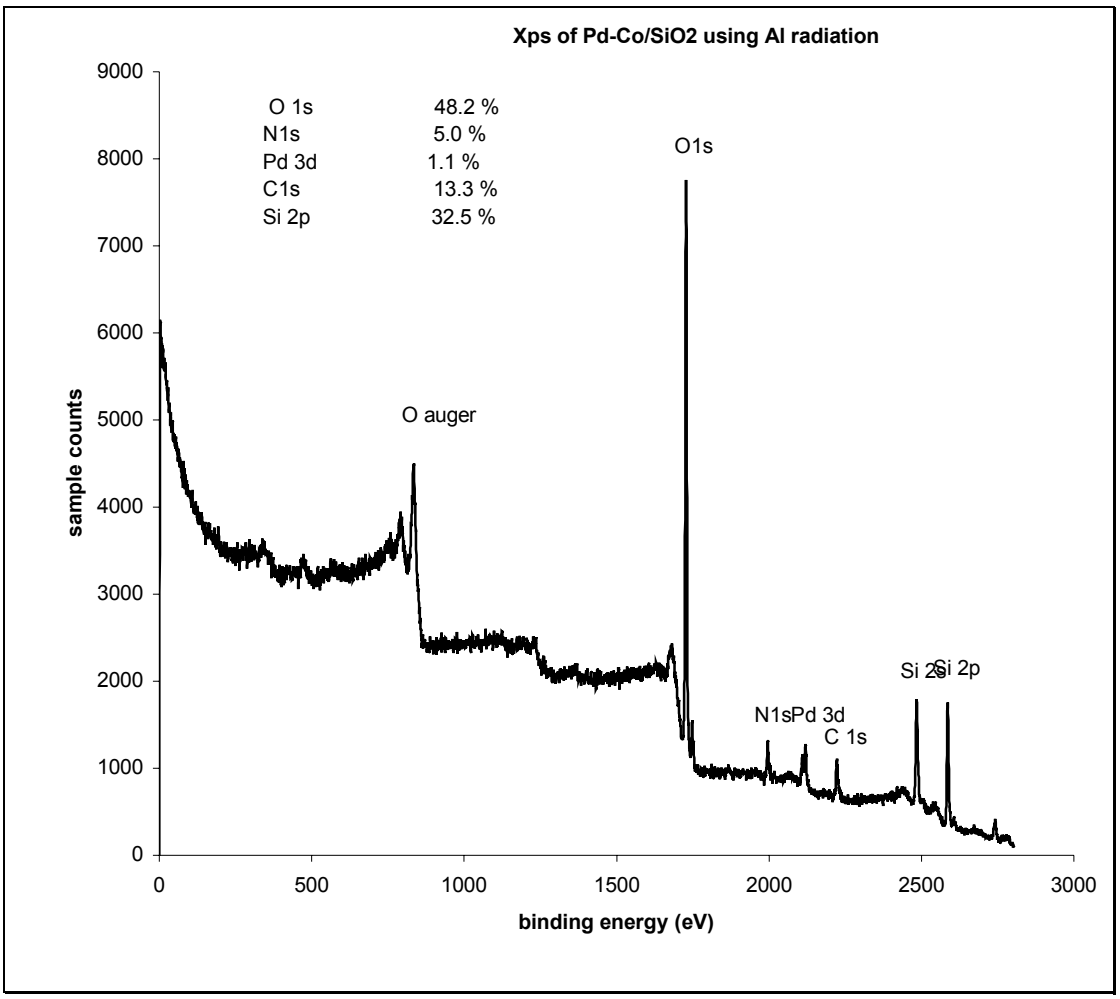

Figure 3. 8 XPS spectrum of Pd-CO/SiO_2 catalyst using Al radiation

Table 3.6 Binding energy (eV) values of Pd-Co/SiO_2 catalyst sample

Element	**O 1s**	**C 1s**	**Pd 3d**	**N 1s**	**Si 2p**
Corrected BE (eV)	540.1	292.6	343.6	406.1	110.6
Experimental BE (eV)	537	289.5	343.6	403	107.5
Atomic %	48.2	13.3	1.1	5.0	32.5

Table 3.7 XPS results of Pd-Co/SiO_2

Sample	**Composition**	**$(Co/Pd)_{bulk}$**	**Co2p, BE in eV**	**Pd 3d, BE in eV**	**$(Co/Si)_{surf}$**	**$(Pd/Si)_{surf}$**	**$(Co/Pd)_{surf}$**
Pd-Co/SiO_2	Pd50Co50	1.00	----	343.6	0	0.033	0

Discussion of XPS results of Pd-Co/SiO_2

The surface compositions of Pd and Co were low when analyzed using XPS. Thus, the presence of the metals on the surface is very negligible, and we can conclude that the surface is composed largely of support silica.

Comparison of bulk and surface ratios of bimetals

Table 3.7 shows the ratio of Co/Pd at the surface and in the bulk. The ratio of Co/Pd at surface is less compared to those of the bulk. In fact this ratio at the surface is negligible, attributed mainly due to not detecting cobalt at the surface. On comparison of Co/Si and Pd/Si ratios at the surface, we see that Pd is more at the surface. Consequently the comparison of Co/Pd in the bulk and Co/Pd at the surface shows that Cobalt species remain more in the bulk of the catalyst. Hence surface segregation of Cobalt can be observed here.

Alloys/Bimetal Formation

Again the formation of alloys are better observed when the catalyst is subjected to oxidative and reductive treatments, and comparing the binding energies of ruthenium and cobalt peak positions. Guczi et al., [42] states in their work about the possibility of formation of bimetallic particles through the TPR results. Later they were able to support the presence of bimetallic particles by studying the core peaks of palladium and cobalt after oxidation/reduction treatments. Thus it is difficult to predict through the XPS results about the formation of bimetallic particles. We have a Pd 3d peak at 343.6 eV. This is far from an alloy observed for Pd_2Si at 336.8 eV. With reference to Si 2p peak at 107.5 eV,

the Pd_2Si peak is observed at 99.6 eV. This states that we are not forming Pd_2Si. Hence our XPS results are inconclusive concerning alloy formation between palladium and silica.

Oxidation state of elements

The Pd 3d binding energy of 343.6 eV after Ar^+ sputter is in close agreement with literature [39]. The Pd $3d_{3/2}$ peak observed at binding energy of 343.6 eV confirms the presence of PdO at the surface [40]. Table 3.8 gives the oxidation state of the elements analyzed by XPS.

Table 3.8 Oxidation states of elements analyzed by XPS

Catalyst	**Element Binding Energy (eV)**	**Oxidation state**
Ru-Co	Ru 3d (281.2)	+2
Pd-Co	Pd 3d (343.6)	+1
Rh-Co	Rh 3d (321.7)	Cannot be determined
Ru-Co	Si 2p (110.6)	+2
Ru-Co	Si 2p (99.2)	+ 2
Rh-Co	Si 2p (116.2)	+2
Rh-Co	Co 2p (778.7)	+1

SEM results

Results of silica support analysis

Figure 3.9 shows the SEM of silica at a magnification of 1500. The image was taken of the substrate to compare with the prepared catalyst surfaces. The resolution is at 20 microns. A similar micrograph is shown for silica at 600 nm in Ono et al. [41].

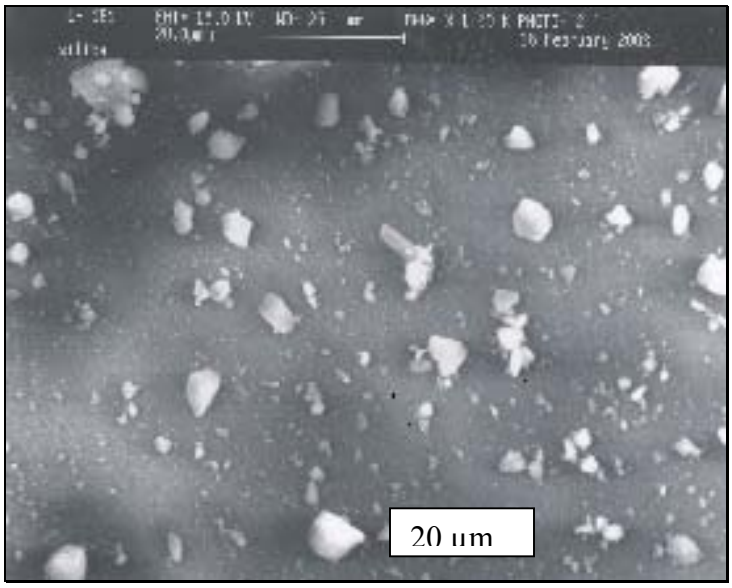

Figure 3.9 SEM of silica surface at 1500x magnification

Results of Pd-Co/SiO_2

A scanning electron microscopy study of a bimetallic Pd-Co/SiO_2 sample was carried out using the Kevex- JEOL scanning electron microscope. Figure 3.11 shows the micrograph of the SEM image with a magnification of 20.

At 2 mm resolution, nothing definitive was observed about the surface particles. The white particles, or particle agglomerates, are evidently due to silica, which is the support for the catalyst. The magnification of the image up to 1500 times shows a better picture, which is shown in Figure 3.10 with a 20-micron resolution. Again the silica particle and the palladium or cobalt particles cannot be distinguished from the image. Palladium and cobalt particles cannot be distinguished. The white colored particles are not due to the metals even though these areas are clearly distinguishable from the rest of the darker particles in the image.

Figure3.10 SEM micrograph of Pd-Co/SiO_2 at 1500X magnification

Figure 3.11 SEM micrograph of Pd-Co/SiO_2 at 20 X magnification

Results of Rh-Co/SiO_2

The SEM analysis for the rhodium -cobalt bimetallic catalyst was also carried out. The obtained micrograph is shown in Figure 3.12 at a resolution of 2 mm. The image has a significant amount of differential charging. Therefore, the sample was subjected to Au sputtering for 2 minutes in Ar+. Figure 3-13 shows the sample after the sputtering.

Figure 3.14 is that of rhodium cobalt bimetallic sample at a greater magnification of 1500 times with a 20-micron resolution. The white particles are clearly distinguishable from the darker ones. The image is that at the surface of silica, but confirmation of the presence of rhodium or cobalt or even silica particles is inconclusive.

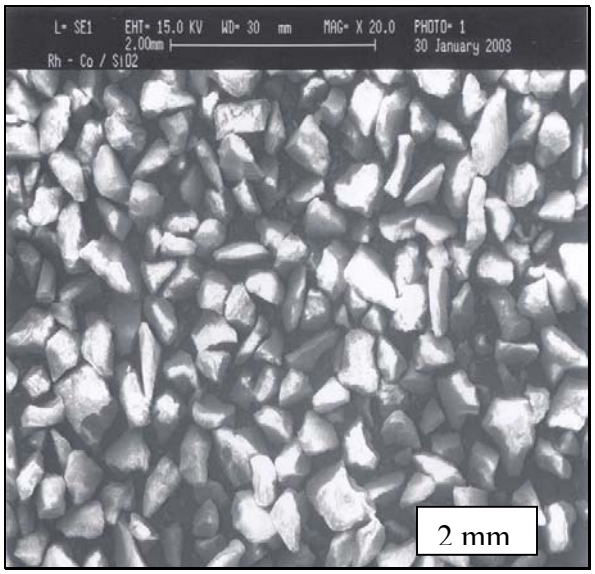

Figure 3.12 SEM micrograph of Rh-Co/SiO_2 at 20x magnification

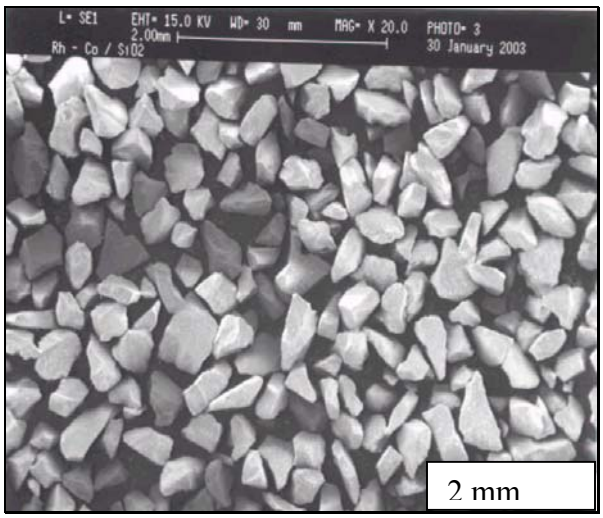

Figure 3.13 SEM micrograph of Rh-Co/SiO_2 at 20x magnification followed by Ar+ sputter

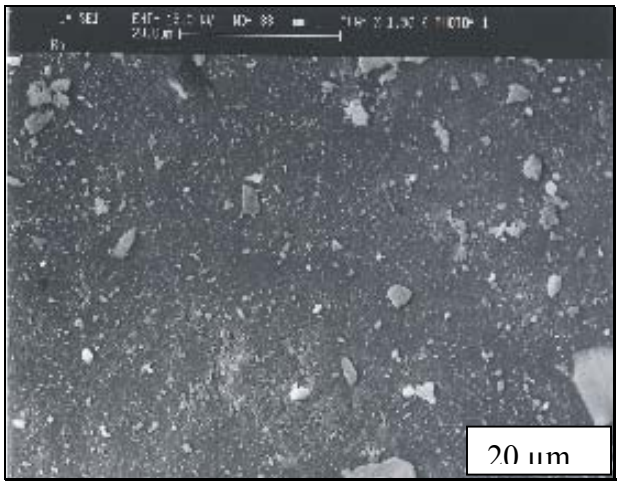

Figure 3.14 SEM micrograph of Rh-Co/SiO_2 at 1500x magnification

Results of Ru-Co/SiO_2

SEM analysis of ruthenium cobalt bimetallic catalyst was initially performed with a magnification of 20, the micrograph is shown in Figure 3.16. Figure 3.15 shows the SEM image micrograph of Ru-Co/SiO_2 at a magnification of 1500X and an image resolution of 20 microns. It is clearly seen that the surface of silica in this sample is smoother compared to those of rhodium or palladium bimetallic samples. The white particles are most distinguishable here, compared to the previous samples. However, confirmation of ruthenium, cobalt, silica or any other surface elements was not possible from SEM images.

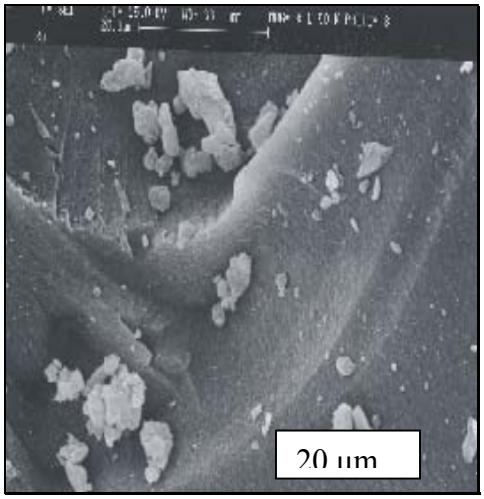

Figure 3.15 SEM micrograph of Ru-Co/SiO_2 at 1500x magnification

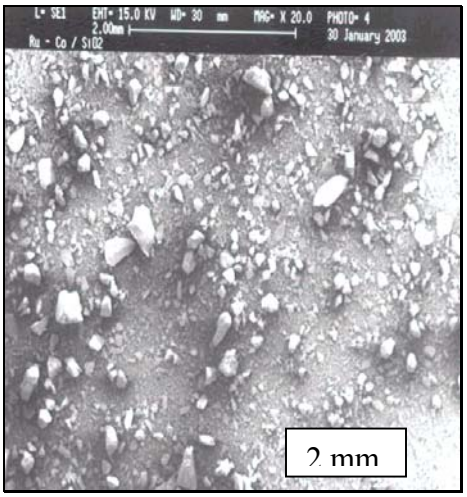

Figure 3.16 SEM micrograph of Ru-Co/SiO_2 at 20x magnification

SEM-EDS analysis of Pd-Co/SiO_2

Analysis for the palladium-cobalt sample was performed using the PGT Excalibur. Figures 3.17, 3.18, and 3.19 show the EDS spectra for the sample at three different positions on the sample. The analysis depth was not changed and remained at about 1-2 microns. The magnification was set at 1500X. Tables 3.9, 3.10, and 3.11 are the data for each of the three image positions. The EDS spectrum for each shows the relative abundances of O and Si compared to the rest of the elements. A notable difference is observed in position # 1, where the palladium peak is comparatively larger. The atomic composition for Pd is more for position #1. A better illustration is shown in Table 3.12 that compares the Pd and Co values for the three positions. A similar observation applies to the Co peak intensity in the spectrum of position # 3. Table 3.13 gives the average composition of the three positions along with calculated error % on a standard deviation from the mean of the compositions.

As most of the peaks here were clearly identifiable, no peaks that could be attributed to any alloys or bimetallic particles were observed. Thus alloy formation was not clearly observed using the SEM-EDS for the Pd-Co catalyst.

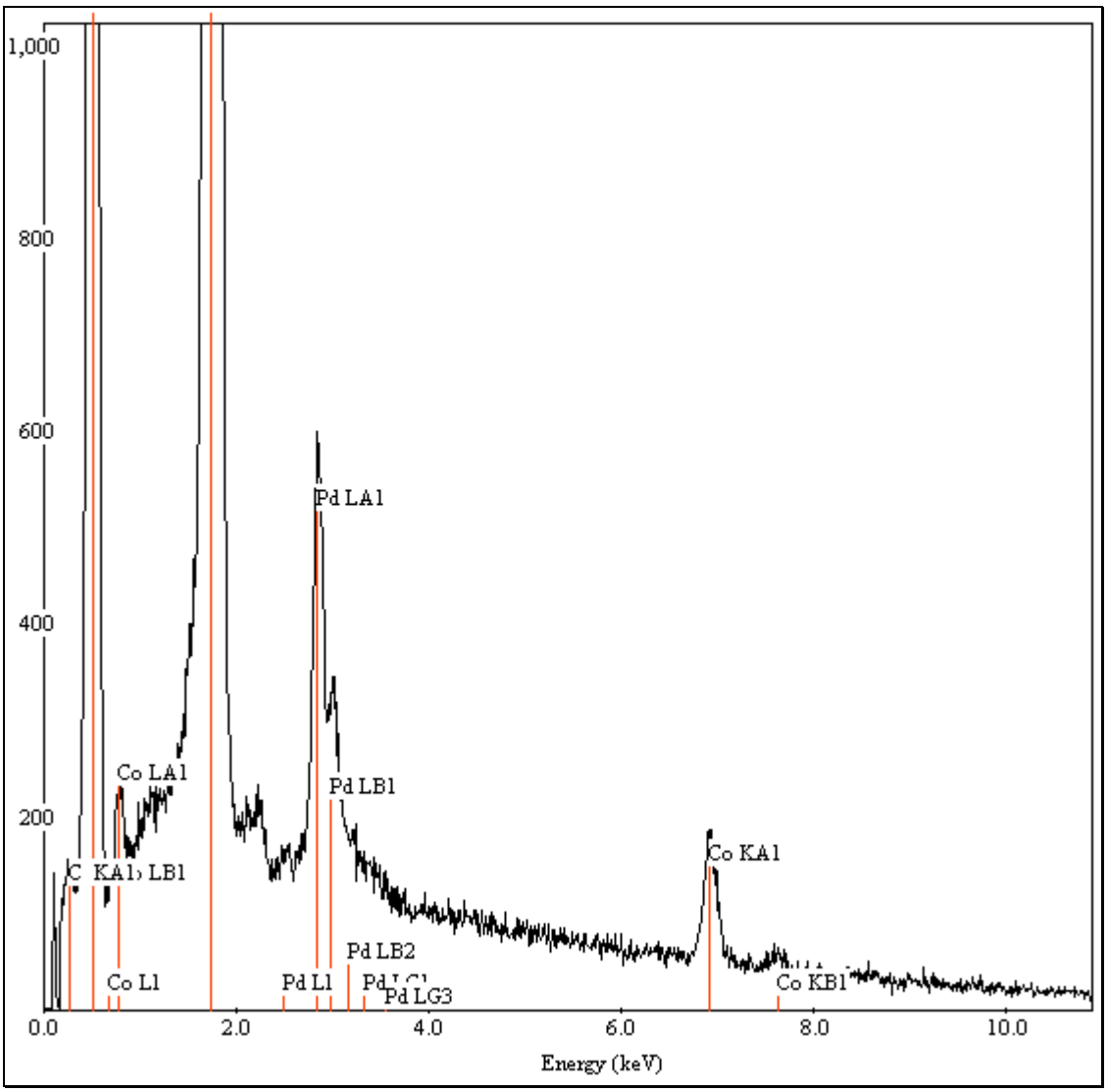

Figure 3.17 SEM-EDS spectrum of position #1

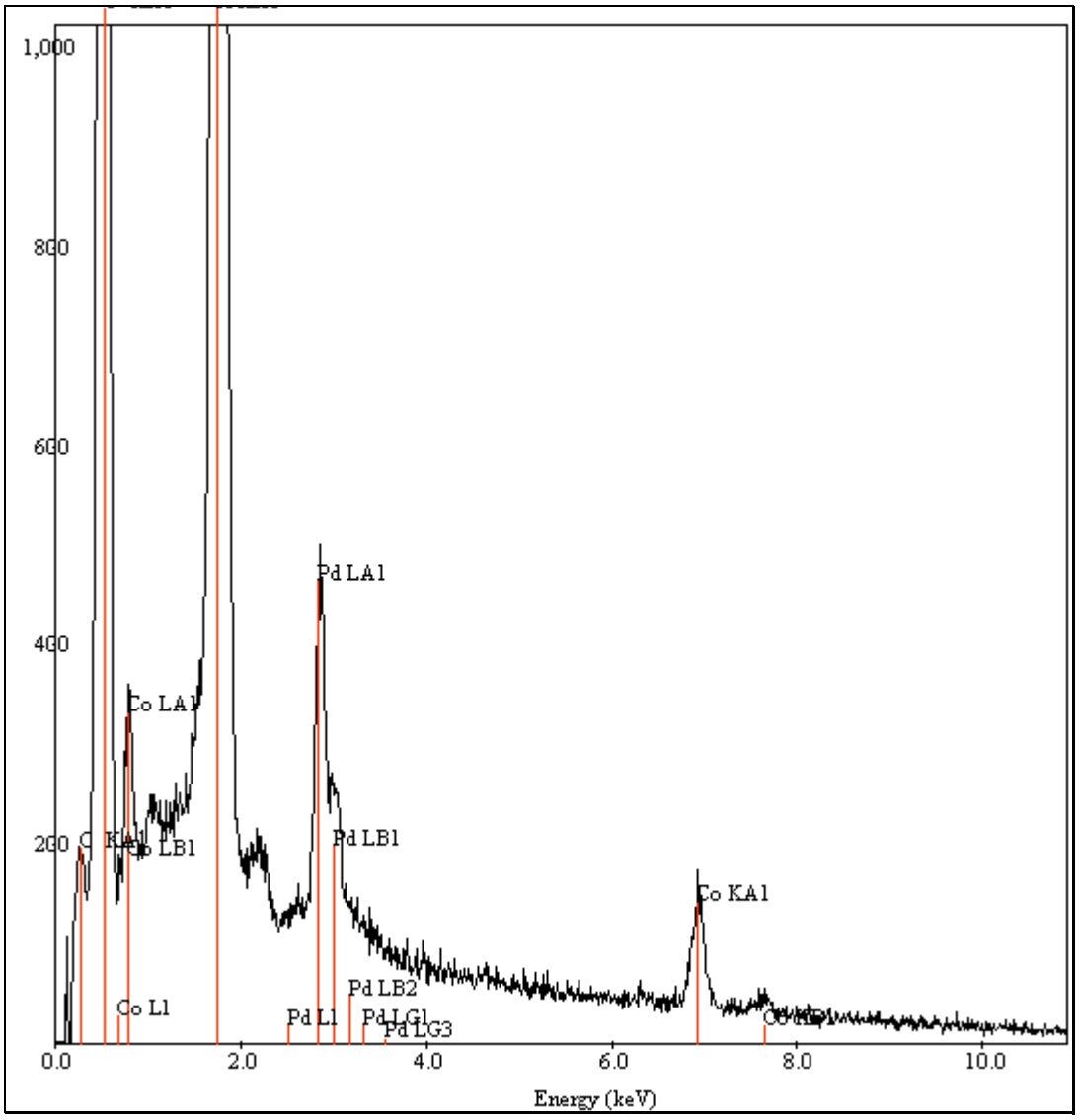

Figure 3.18 SEM-EDS spectrum of position #2

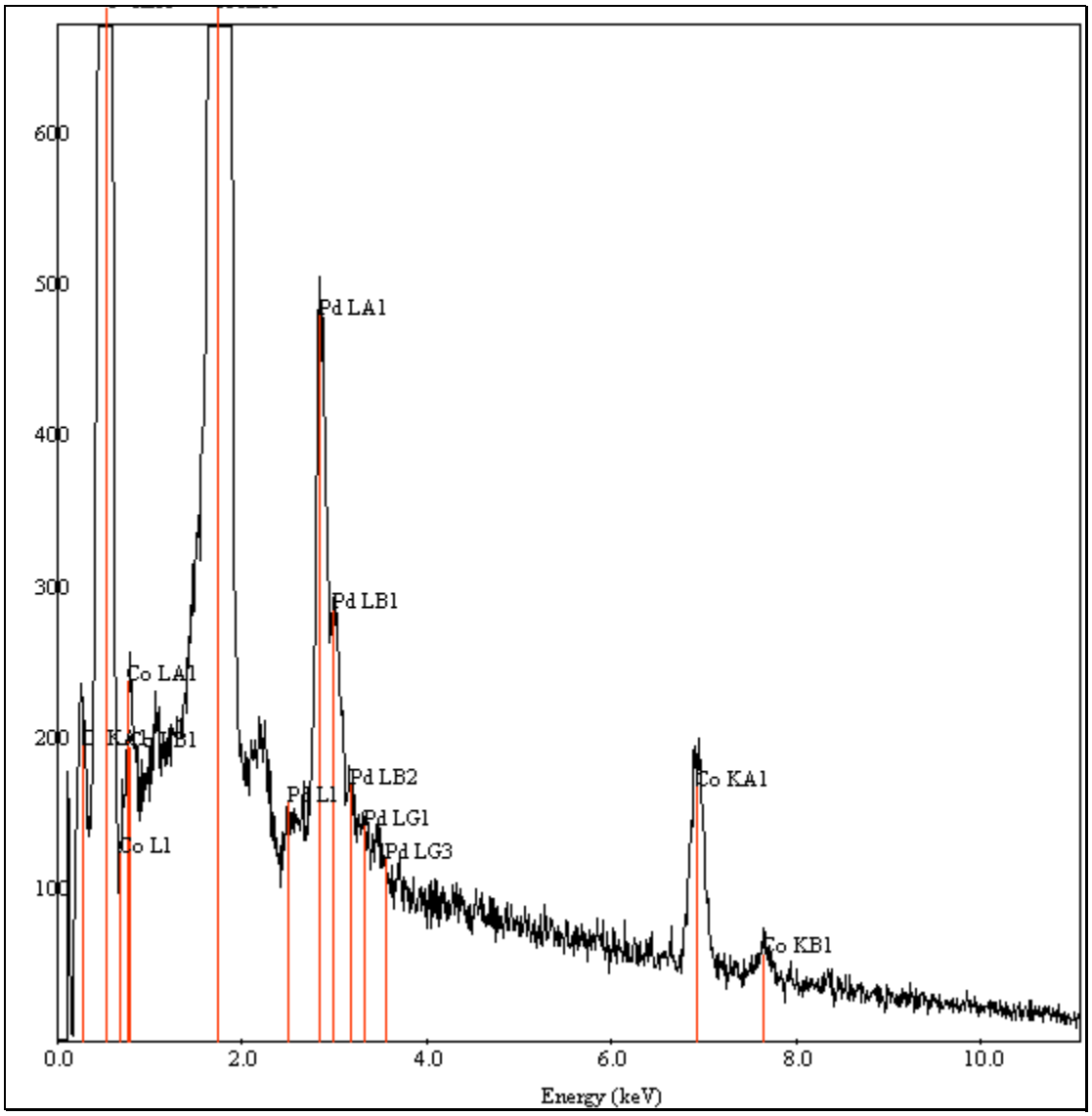

Figure 3.19 SEM-EDS spectrum of Pd-Co/SiO_2 for position #3

Table 3.9 SEM-EDS data for Pd-Co/SiO_2 for above image position # 1

Element	Weight %	Atomic %	Compound weight %
O	32.831	45.719	32.831
Si	56.713	44.991	56.713
Co	2.027	0.766	2.027
C	4.107	7.619	4.107
Pd	4.323	0.905	4.323
Total	100.00	100.00	100.00

Table 3.10 SEM-EDS data for Pd-Co/SiO_2 for above image position # 2

Element	Weight %	Atomic %	Compound weight %
O	41.445	54.405	41.445
Si	48.852	36.533	48.852
Co	1.925	0.686	1.925
C	4.409	7.711	4.409
Pd	3.368	0.665	3.368
Total	100.00	100.00	100.00

Table 3.11 SEM-EDS data for Pd-Co/SiO_2 for above image position # 3

Element	Weight %	Atomic %	Compound weight %
O	34.753	46.641	34.753
Si	52.493	40.133	52.493
Co	2.618	0.954	2.618
C	6.448	11.528	6.448
Pd	3.688	0.744	3.688
Total	100.00	100.00	100.00

Table 3.12 Atomic percentage comparison of Co and Pd for the three positions

Element	Position # 1	Position # 2	Position # 3
Co	0.766	0.686	0.954
Pd	0.905	0.665	0.744

Table 3.13 SEM-EDS data for Pd-Co/SiO_2 showing average of three positions

Element	Weight %	Std Error %	Atomic %	Std Error %	Compound weight %	Std Error %
O	36.343	2.610	48.921	2.754	36.343	2.610
Si	52.686	2.271	40.552	2.450	52.686	2.271
Co	2.190	0.216	0.802	0.079	2.190	0.216
C	4.988	0.735	8.952	0.287	4.988	0.735
Pd	3.793	1.287	0.7713	0.280	3.793	1.287
Total	100.00		100.00		100.00	

SEM-EDS analysis of Rh-Co/SiO_2

Analysis for the rhodium-cobalt sample was performed using the PGT Excalibur. Figures 3.20, 3.21, and 3.22 show the EDS spectra for the sample at three different positions of the sample image. The analysis depth was not changed and remained at about 1-2 microns. The magnification was set at 1500X, and other than position # 2, the images didn't show much differential charging. Tables 3.14, 3.15, and 3.16 are the data for each of the three image positions. The EDS spectrum for each shows the relative abundance of O and Si compared to the rest of the elements. A notable difference is observed in position # 2, where the rhodium peak is comparatively small. The atomic composition is less for position #2. A better illustration is shown in Table 3.18 that compares the Rh and Co values for the three positions. A similar observation applies for Co peak intensity in spectrum of position # 2. A small peak attributed to Na is shown for position # 1, but the composition was too low for any significant compositional information. Table 3.17 gives the average composition of the three positions along with calculated error % on a standard deviation from the mean of the compositions.

As most of the peaks here were clearly identifiable, no peaks that could be attributed to any alloys or bimetallic particles were observed. Thus, alloy formation was not clearly observed using the SEM-EDS for the Rh-Co catalyst.

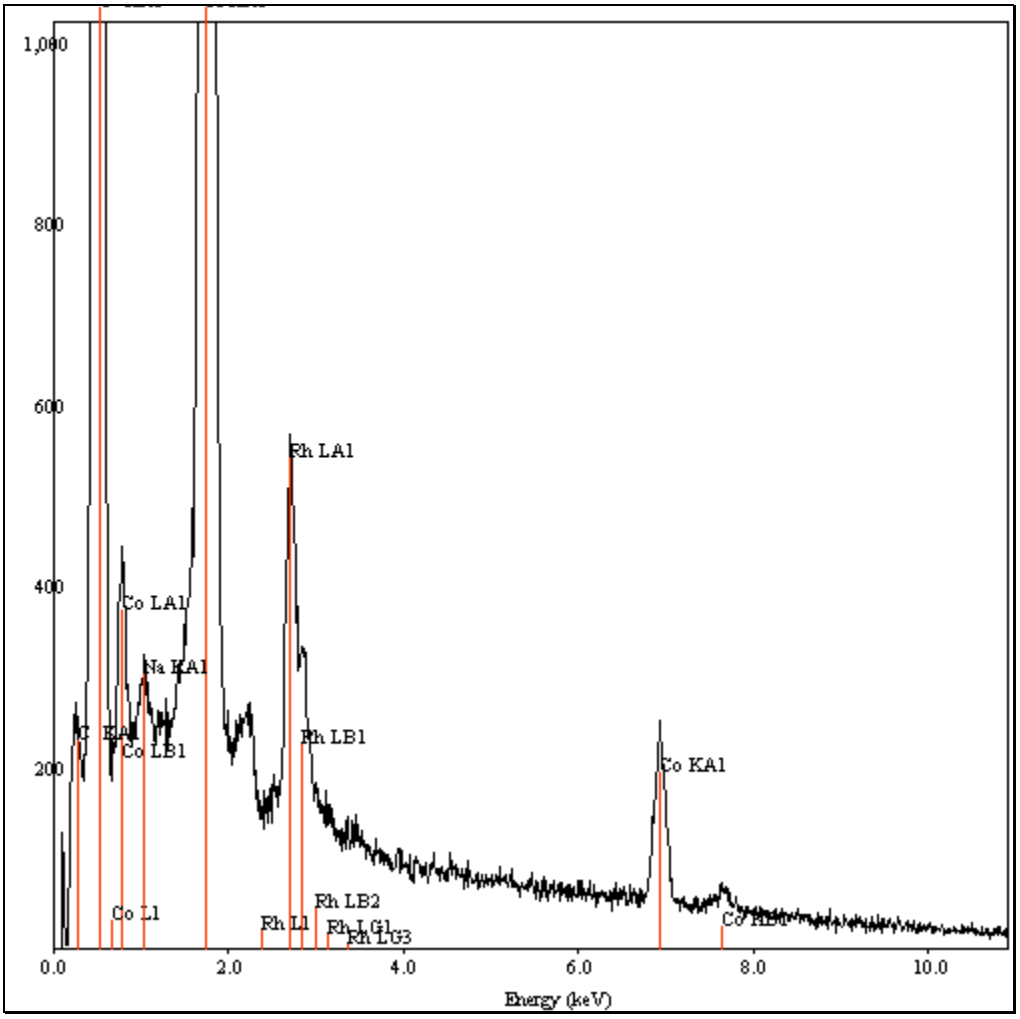

Figure 3.20 SEM-EDS spectrum of position #1

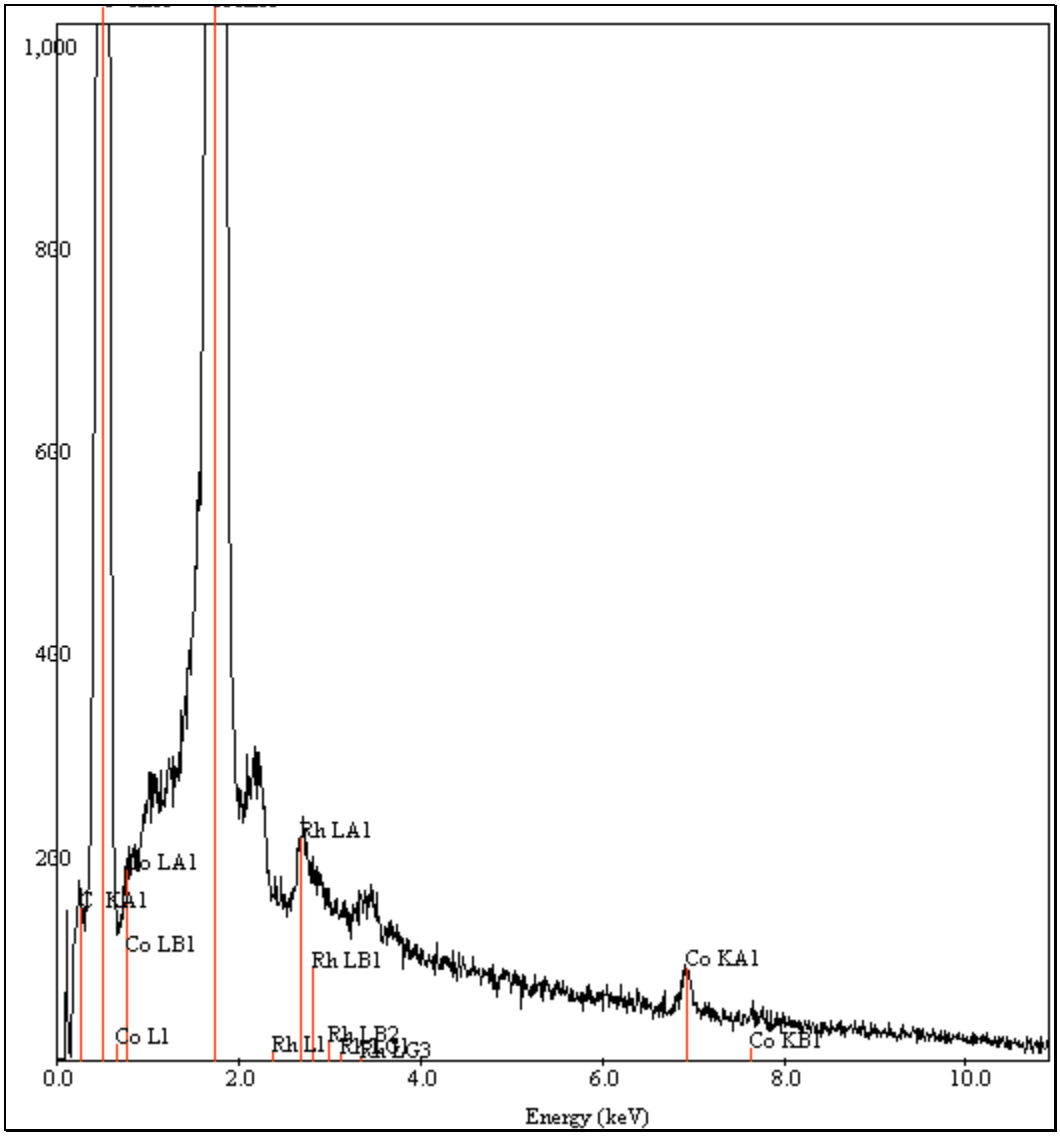

Figure 3.21 SEM-EDS spectrum of Rh-Co/SiO_2 for position #2

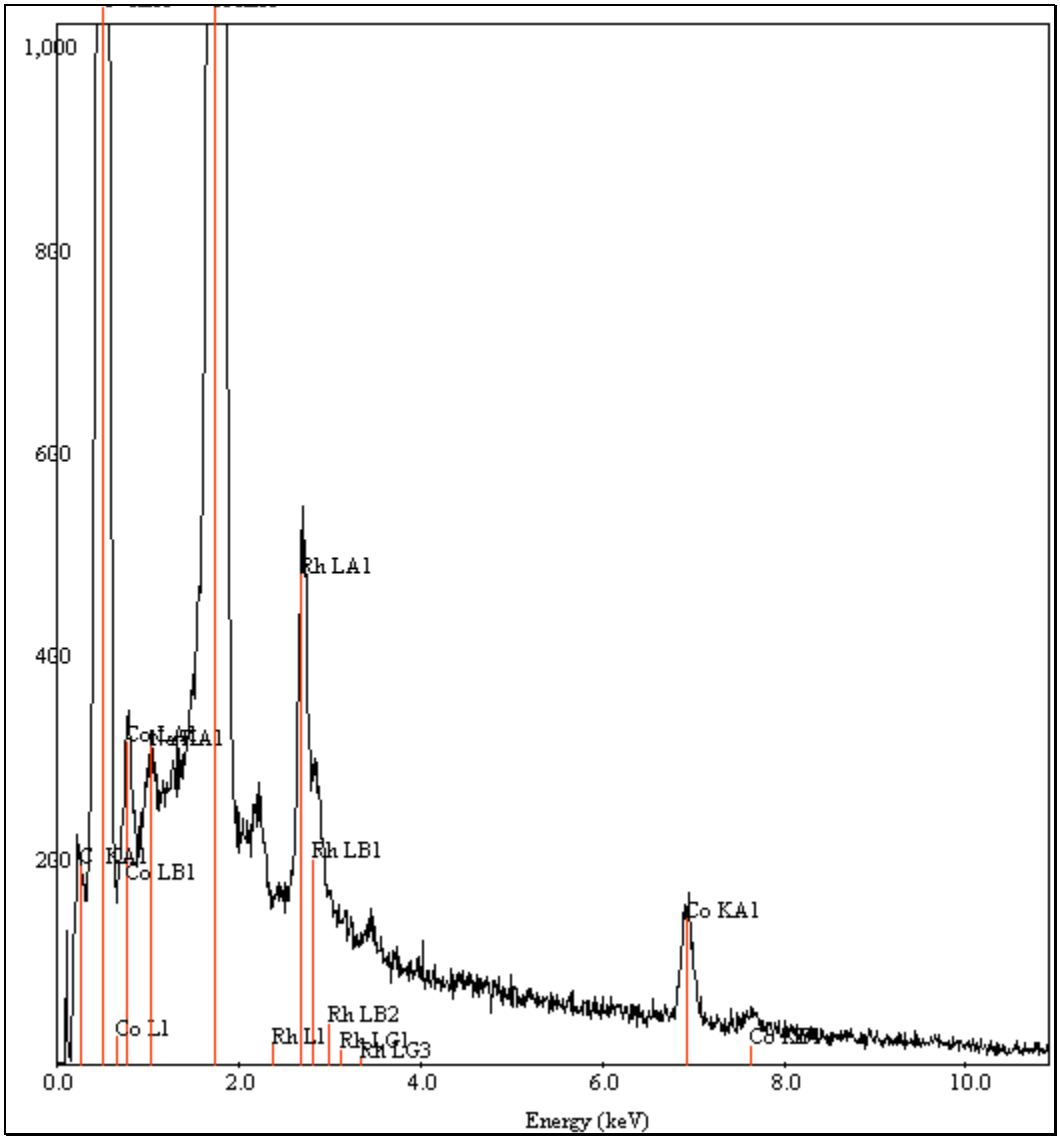

Figure 3.22 SEM-EDS spectrum of Rh-Co/SiO_2 position # 3

Table 3.14 SEM-EDS data for Rh-Co/SiO_2 for image position # 1

Element	Weight %	Atomic %	Compound weight %
O	40.309	53.154	40.309
Si	50.228	37.731	50.228
Co	1.635	0.585	1.635
Rh	3.138	0.643	3.138
C	4.270	7.501	4.270
Na	0.421	0.386	0.421
Total	100.00	100.00	100.00

Table 3.15 SEM-EDS data for Rh-Co/SiO_2 for image position # 2

Element	Weight %	Atomic %	Compound weight %
O	36.552	48.722	36.552
Si	59.096	44.875	59.096
Co	0.435	0.158	0.435
Rh	0.453	0.094	0.453
C	3.464	6.151	3.464
Total	100.00	100.00	100.00

Table 3.16 SEM-EDS data for Rh-Co/SiO_2 for image position # 3

Element	Weight %	Atomic %	Compound weight %
O	34.753	46.641	34.753
Si	52.493	40.133	52.493
Co	2.618	0.954	2.618
C	6.448	11.528	6.448
Pd	3.688	0.744	3.688
Total	100.00	100.00	100.00

Table 3.17 SEM-EDS data for Rh-Co/SiO_2, showing average of the three positions

Element	Weight %	Std. Error %	Atomic %	Std. Error %	Compound weight %	Std Error %
O	39.6893	1.6616	52.242	1.8268	39.6893	1.6616
Si	51.665	3.941	38.806	3.238	51.665	3.941
Co	1.6176	0.677	0.575	0.237	1.6176	0.677
Rh	2.3766	0.968	.484	0.196	2.3766	0.968
C	4.3503	0.536	7.619	0.8835	4.3503	0.536
Na	0.421	0.03	0.386	0.024	0.421	0.03
Total	100.00		100.00		100.00	

Table 3.18 Atomic percentage comparison of Co and Rh for the three positions

Element	Position # 1	Position # 2	Position # 3
Co	0.982	0.158	0.585
Rh	0.715	0.094	0.643

SEM-EDS analysis of Ru-Co/SiO_2

Analysis for the ruthenium-cobalt sample was performed using the PGT Excalibur. Figures 3.23, 3.24 and 3.25 shows the EDS spectra for the sample at three different positions of the sample image. The analysis depth was not changed and remained at about 1-2 microns. The magnification was set at 1500. Tables 3.19, 3.20, and 3.21 are the data for each of the three image positions. The EDS spectrum for each shows the relative abundance of O and Si compared to the rest of the elements. A notable difference is observed in position # 3, where the ruthenium peak is comparatively larger. The atomic composition for Ru is more for position #3. A better illustration is shown in Table 3.22 that compares the Ru and Co values for the three positions. A similar observation applies for the Co peak intensity in spectrum of position # 2. Table 3.23 gives the average composition of the three positions along with calculated error % on a standard deviation from the mean of the compositions.

As most of the peaks here were clearly identifiable, no peaks that could be attributed to any alloys or bimetallic particles were observed. Thus alloy formation was not clearly observed using the SEM-EDS for the Ru-Co catalyst.

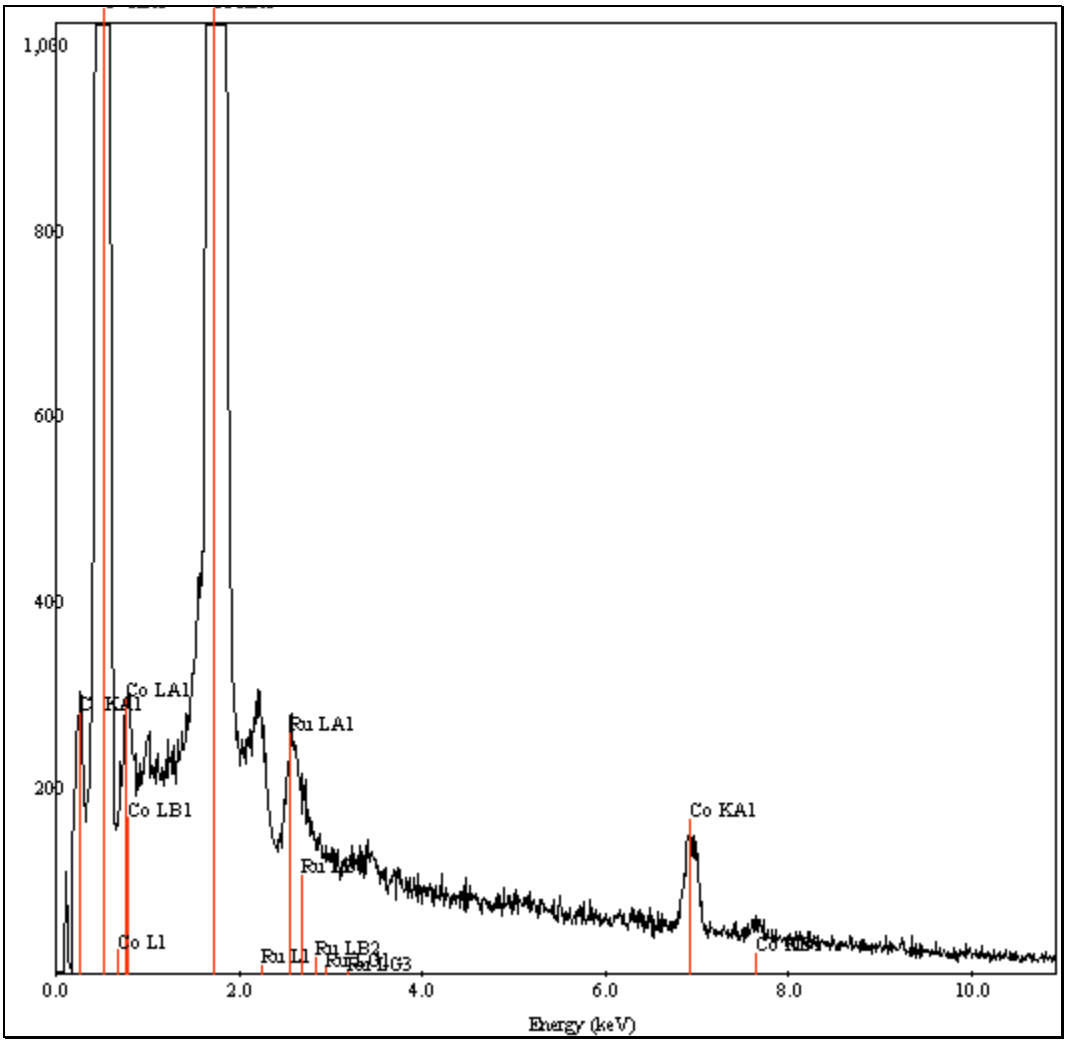

Figure 3.23 SEM-EDS spectrum of Ru-Co/SiO_2 for position # 1

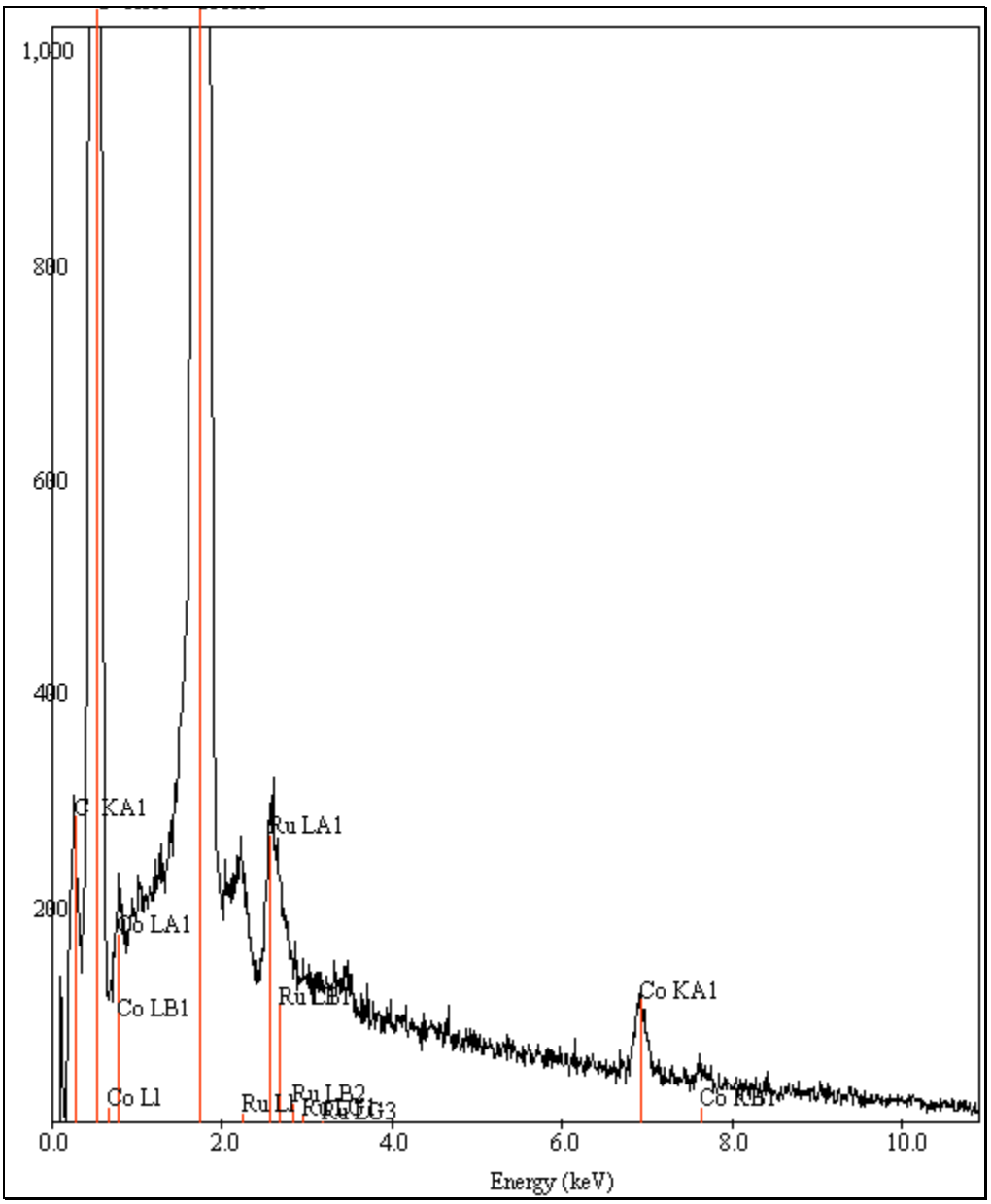

Figure 3.24 SEM-EDS spectrum of Ru-Co/SiO_2 for position # 2

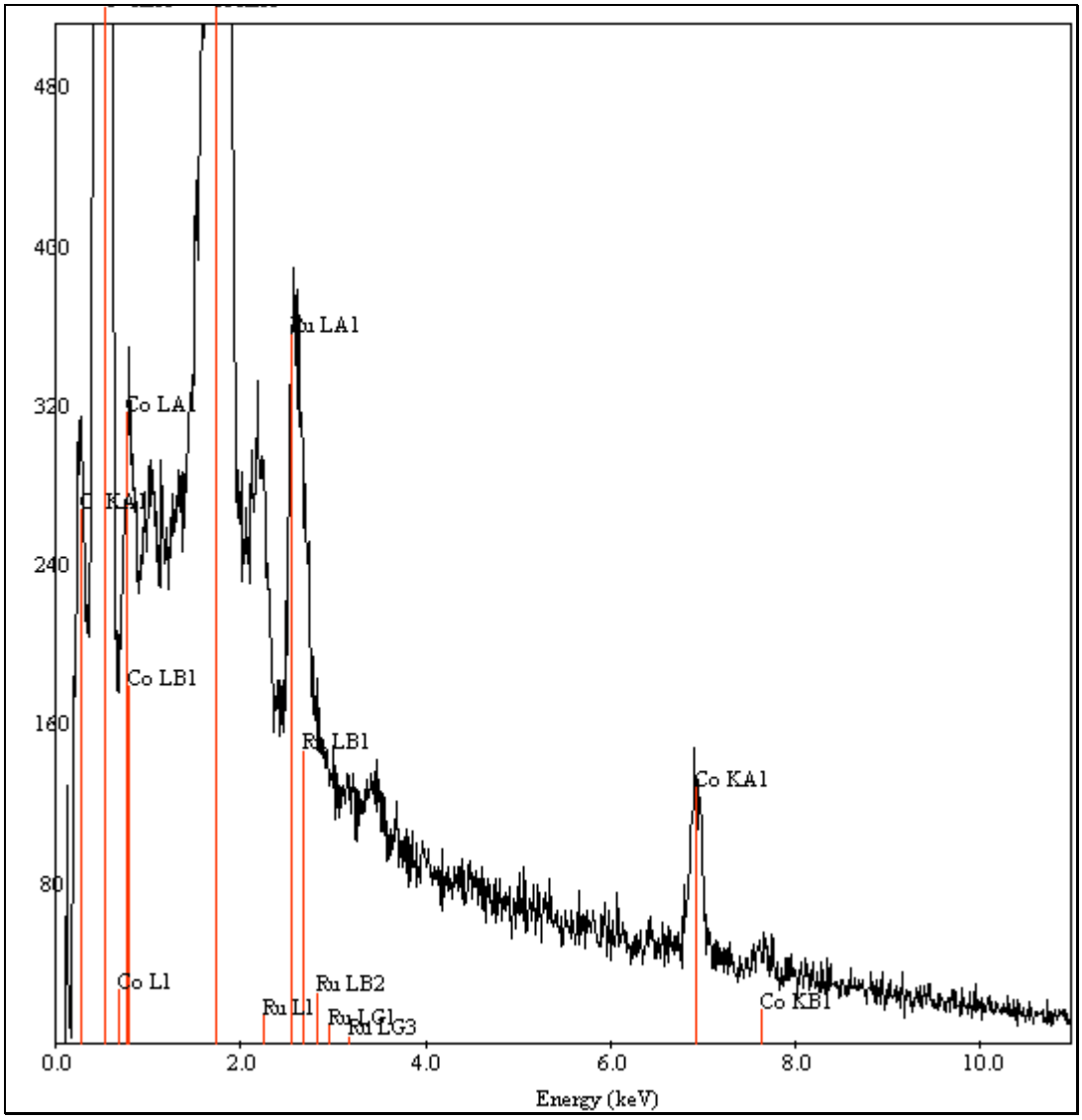

Figure 3.25 SEM-EDS spectrum of Ru-Co/SiO_2 for position #3

Table 3.19 SEM-EDS data for Ru-Co/SiO_2 for above image position # 1

Element	Weight %	Atomic %	Compound weight %
O	41.105	51.861	41.105
Si	49.066	35.266	49.066
Co	1.632	0.559	1.632
C	7.208	12.116	7.208
Ru	0.989	0.198	0.989
Total	100.00	100.00	100.00

Table 3.20 SEM-EDS data for Ru-Co/SiO_2 for image position #2

Element	Weight %	Atomic %	Compound weight %
O	36.306	47.044	36.306
Si	54.423	40.173	54.423
Co	1.044	0.367	1.044
C	7.053	12.175	7.053
Ru	1.173	0.241	1.173
Total	100.00	100.00	100.00

Table 3.21 SEM-EDS data for Ru-Co/SiO_2 for the image position # 3

Element	Weight %	Atomic %	Compound weight %
O	43.363	54.742	43.363
Si	47.879	34.433	47.879
Co	1.107	0.379	1.107
C	6.016	10.119	6.016
Ru	1.634	0.327	1.634
Total	100.00	100.00	100.00

Table 3.22 Atomic Percentage comparison of Co and Ru for the three positions

Element	Position # 1	Position # 2	Position # 3
Co	0.559	0.367	0.585
Ru	0.198	0.241	0.327

Table 3.23 SEM-EDS data for Ru-Co/SiO_2 showing average of the three image positions

Element	Weight %	Std Error %	Atomic %	Std Error %	Compound weight %	Std Error %
O	40.258	2.080	51.2156	2.2455	40.258	2.080
Si	50.456	2.012	36.624	1.790	50.456	2.012
Co	1.261	0.186	0.435	0.062	1.261	0.186
C	6.759	0.374	11.470	0.675	6.759	0.374
Ru	1.265	0.191	0.2553	0.037	1.265	0.191
Total	100.00		100.00		100.00	

Comparison of results of XPS and SEM-EDS

The surface characterization of the bimetallic catalysts using XPS and the SEM-EDS methods are compared here to give a better representation of the surface composition of the elements at different analysis depths. For the XPS the analysis depth may be estimated by $d = \lambda \sin\theta$ **(11)**

Where d is the analysis depth, λ is the inelastic mean free path, and θ is the take-off angle of the analyzed electrons.

The analysis depth used for the XPS was between 1-100 Angstroms, while those for the EDS analysis stood between 500-1000 Angstrom units. Thus EDS, analyzes to a greater depth within the bulk of the catalyst. The Tables 3.24, 3.25, and 3.26 shows the comparison of XPS with EDS measurements for the three bimetallic catalysts. AD is the analysis depth denoted in the tables.

For XPS, 5 percent nitrogen was found in the palladium-cobalt catalyst. The cobalt percentage in Pd-Co catalyst by XPS was zero, while it is found to be 0.8 using EDS. This can be attributed to that the greater analysis depth, employed in EDS. XPS provides information on cobalt segregation into the bulk of the catalyst. Similarly for Palladium, Rhodium and Ruthenium the SEM results indicate these species to be present in the bulk. Hence surface segregation is observed for all the three metals.

Table 3.24 XPS and SEM-EDS comparison of elements in Pd-Co/SiO_2 catalyst

Element Atomic %	Pd	Co	Si	C	O	N
XPS, AD= 100 Å	1.1	0.0	32.5	13.3	48.2	5.0
EDS, AD = 1000 Å	0.7	0.8	40.5	8.9	48.9	0.0

AD = Analysis Depth.

Table 3.25 XPS and SEM-EDS comparison of elements in Rh -Co/SiO_2 catalyst

Element Atomic %	Rh	Co	Si	C	O	N
XPS, AD= 100 Å	0.4	0.3	30.6	12.2	56.5	0.0
EDS, AD = 1000 Å	0.5	0.5	38.8	7.6	52.2	0.0

AD = Analysis Depth

Table 3.26 XPS and SEM-EDS comparison of elements in Ru -Co/SiO2 catalyst

Element Atomic %	**Ru**	**Co**	**Si**	**C**	**O**	**N**
XPS, AD= 100 Å	0.7	0.3	32.9	4.3	61.8	0.0
EDS, AD = 1000 Å	0.2	0.4	36.6	11.5	51.2	0.0

AD = Analysis Depth

Physisorption results for silica

The physisorption analysis on silica was carried out in a Quantachrome Autosorb Automated Gas Sorption System. The silica was degassed prior to the experiment for 6 hours at a temperature of 300^0C. Table 3.27 shows the various operating conditions for the experiment. Table 3.28 shows the results obtained for silica specific surface area using different physisorption methods. The BET method was used exclusively in this study.

The specific surface area was calculated based on the Multipoint BET theory of nitrogen adsorption. The temperature of the liquid nitrogen bath is 77 K, which is the temperature at which nitrogen adsorbs on to the surface of silica. Figure 3.29 shows the Multipoint BET plot obtained for silica. Based on the slope of the straight line and its intercept, the weight of a monolayer of nitrogen adsorption on silica surface was obtained. The surface area was calculated using the values of Avogadro's number, molecular weight of the adsorbate and the cross sectional area of a nitrogen molecule. The specific surface area is obtained through the knowledge of the silica amount used.

The importance of measuring the pore volume and specific surface area lies in the preparation of the three bimetallic catalysts. The pore volume of the support is an important factor when preparing catalysts using the impregnation method. Thus, with the knowledge of the pore volume, the amount of the bimetallic precursors that must be used to prepare a particular weight percent catalyst can be obtained. Value of 1.101 cc/g for pore volume and 304.4 m^2/g for the surface area were determined from experimental data and are in accordance with the data given by the manufacturer.

Table 3.27 Operating conditions for nitrogen adsorption on silica

Sample Weight	0.1089 grams
Adsorbate	Nitrogen
Cross-section area	16.2 A^2/molecule
Molecular weight	28.0134 g/mol
Outgas Temperature	300.0 deg c
Outgas Time	6.0 hours
P/P_0 tolerance	2
Equilibrium Time	5
Bath Temperature	77.35 K
Analysis Time	898.5 min

Table 3.28, Specific Surface area and pore volume results for silica

Multipoint BET	**304.4 m^2/g**
Adsorption Pore Volume	**1.101 cc/g**

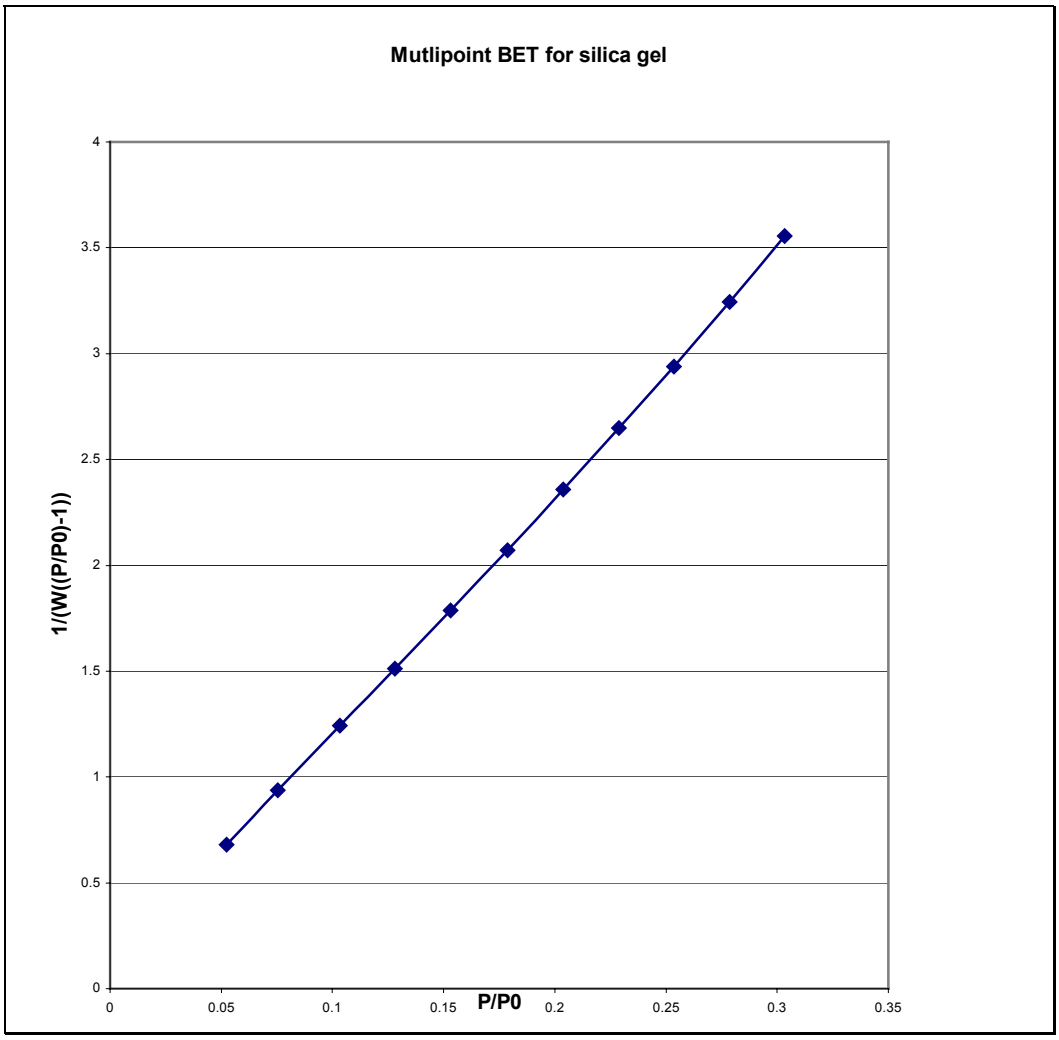

Figure 3. 26 BET plot for silica

TPR Results

TPR analysis of Pd-Co/SiO_2

Temperature-programmed reduction experiments were done on the Pd-Co catalyst using the Autochem 2910 instrument. The weight of the catalyst was approximately 0.1017 grams. A mixture of hydrogen and argon (10.2%) at the rate of 50 cc /min was used with the temperature starting from ambient temperature up to 425^0C. The ramping rate for the experiment was set at 5 deg C/min.

The TPR plot is shown in Figure 3.27. The result of the TPR plot shows only one significant peak at 343 K. The composition of the prepared catalyst is 50 % Co and 50 % Pd, with a theoretical Co/Pd ratio of 1.0. However, the surface Co/Pd ratio is zero as obtained from XPS. The percentage of palladium analyzed by XPS is 1.1 and that of cobalt almost zero. Hence, TPR results would be consistent with only palladium at the surface.

Generally with low metal loadings of Pd and Co, with Pd at 5%, there arise difficulties in studying the TPR spectra at such low concentrations [42]. At such low concentrations, the interactions between both the metals palladium and cobalt are minimal, and only very small amounts of cobalt are reduced, in addition to an entire reduction of palladium. The TPR peak spectra confirm this supposition. The peak observed at 70^0C is that for reduction of PdO to Pd, but this reduction was reported to be at 150^0C in literature [42] for 5 % metal loading of 50 % Co and 50 % Pd catalyst prepared by sol/gel method. The reduction of cobalt oxide usually takes place at

temperatures around 350^0C-450^0C [42] but no reduction peaks for cobalt oxide were identified. This is attributed to the low concentrations of cobalt oxide at the surface.

Juszcyk at al. [24] discusses alloy formation in Pd-Co/SiO_2 catalysts. For well-mixed Pd-Co alloys one should not expect any formation of a β-hydride phase during TPR, [24] since both alloy components Pd and Co, are separated. Guczi et al. [42] discusses bimetallic particle formation in their paper, stating that the formation of a shoulder peak for the TPR study of Pd-Co/SiO_2 on addition of palladium to cobalt indicates the presence of bimetallic particles. The presence of a single peak with no shoulder suggests that bimetallic particles were not formed in this work. Another aspect is the shift of the cobalt peak on addition of palladium, and the peak widening of palladium, indicating palladium dispersion [42].

.

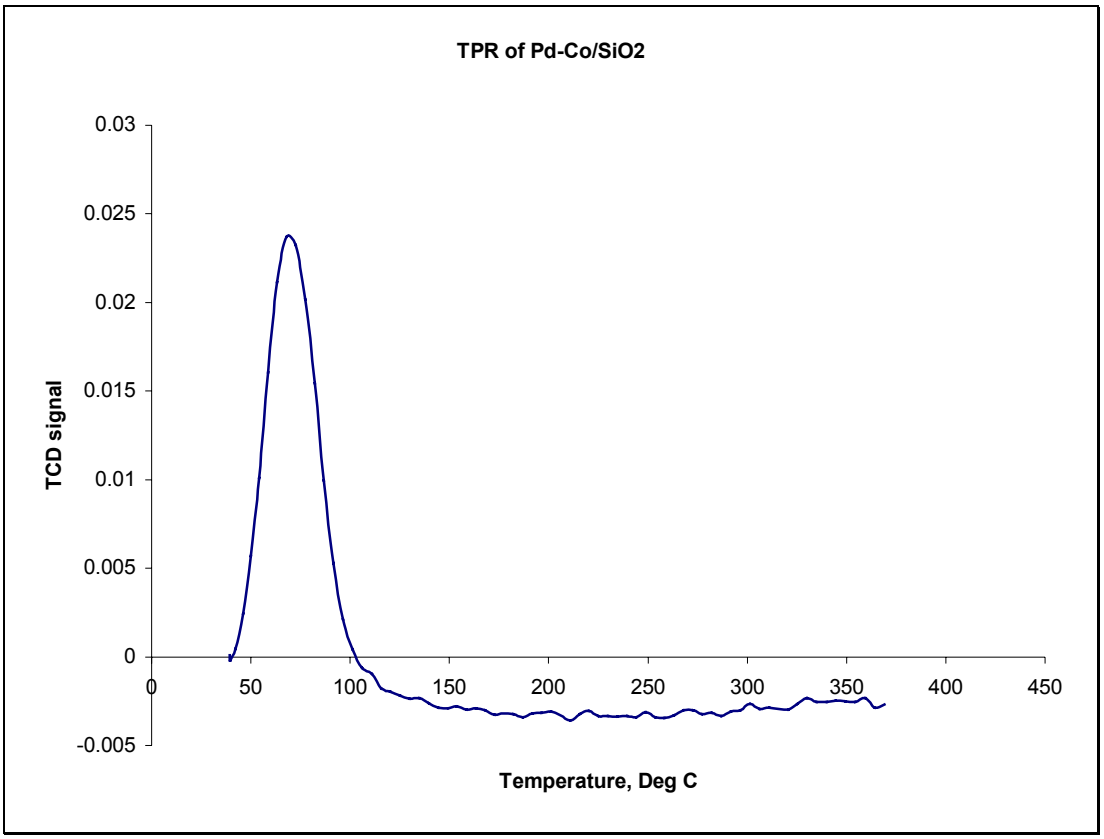

Figure 3. 27 TPR of Pd-Co on SiO_2 support

TPR analysis of Rh-Co/SiO_2

The temperature-programmed reduction was performed on the Rh-Co catalyst using the Autochem 2910 instrument. The weight of the catalyst used to measure was approximately 0.0668 grams. A mixture of hydrogen and argon (10.2%) at a rate of 25 cc /min was used with the temperature starting from ambient temperature up to 425^0C. The ramping rate for the experiment was set at 5^0C/min.

The TPR plot is shown in Figure 3.29. The result of the TPR plot shows only one significant peak at 77^0C. The composition of the prepared catalyst is 50 % Co and 50 % Rh, with a theoretical Co/Rh ratio of 1.0. Blik et al. [43] did work on similar Rh-Co/SiO_2 catalysts. 5 percent weight of metal, with Co: Rh=1:1 atomic ratio were prepared using similar catalyst preparation techniques. They also reported a peak at 95^0C, which is the reduction of Rh_2O_3. Thus it is concluded that the reduction peak at 77^0C in this study is that of rhodium oxide reduction to rhodium.

The reduction peaks of Co usually lies between 200-700^0C as reported earlier [43]. But no reduction peak for cobalt is seen in the results. As a result it is concluded that there is no formation of Rh-Co alloys or bimetallic particles for these catalysts. XPS measurements showed that surface concentrations of Rh and Co were both 0.4 and 0.3 %, respectively.

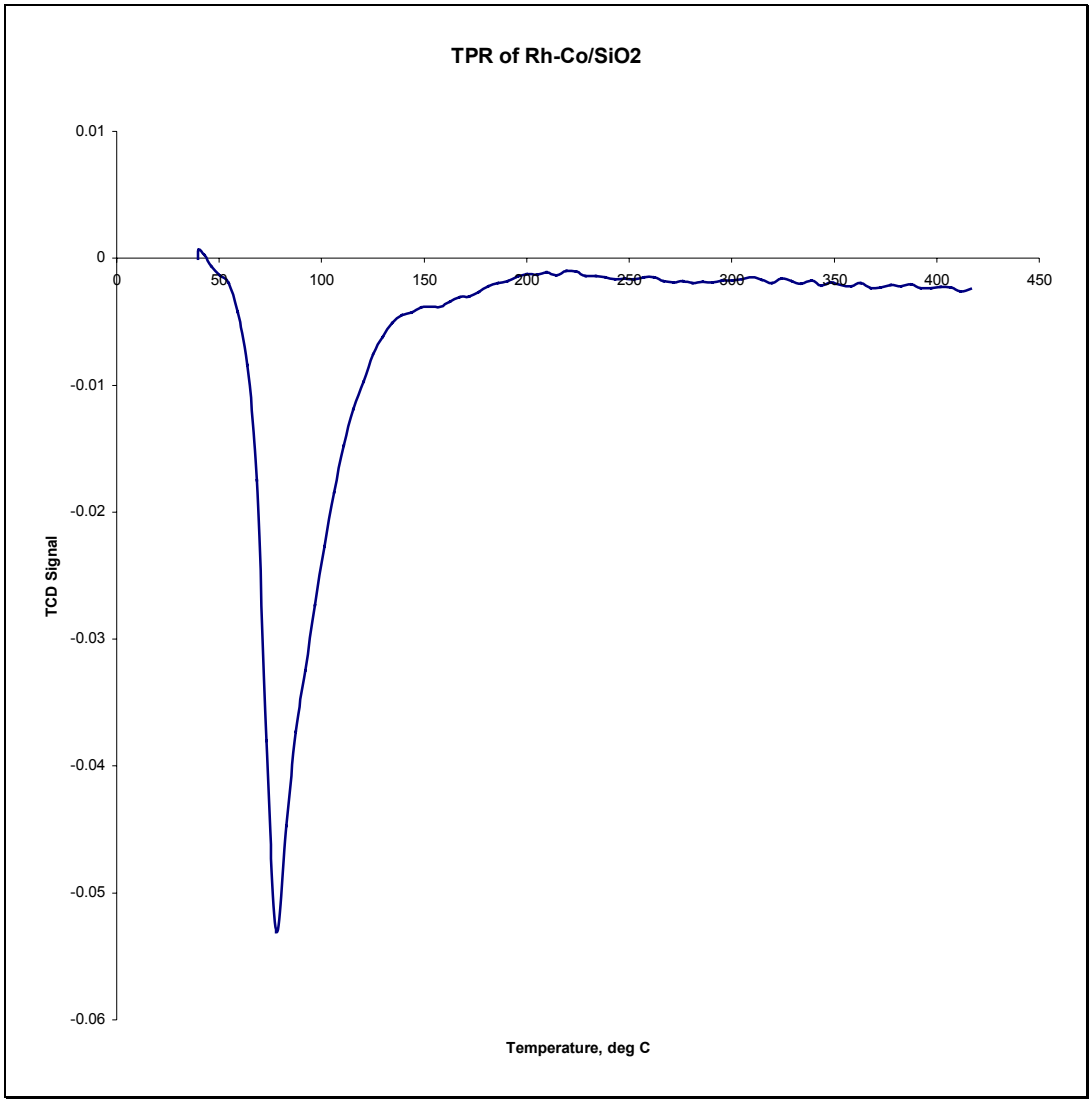

Figure 3.28 TPR of Rh-Co on SiO_2 support

TPR analysis of Ru-Co/SiO_2

Temperature-programmed reduction was performed on the Ru-Co catalyst using the Autochem 2910 instrument. The weight of the catalyst used was approximately 0.1028 grams. A mixture of hydrogen and argon (10.2%) at the rate of 25 cc /min was used with the temperature starting from ambient temperature up to 425 deg C. The ramping rate for the experiment was set at 5deg C/min.

The TPR plot is shown in Figure 3.31. Two reduction peaks are observed. The first occurred at 133^0C and the second one was a very small shoulder peak observed at 204^0C. The second small peak at 204^0C must be the TPR of bimetallic Ru-Co particles [44]. Thus it confirms that the reduction peak at 204^0C in our study is that of the reduction of a bimetallic particle of Ru and Co. The reduction peak for rhodium is at 230^0C as shown in published results [44] and [20].

The peak at 133^0C is confusing at this point. Since reduction peak for ruthenium occurs at around 230^0C, this peak is not that of ruthenium oxide reduction. The reduction peaks for cobalt are again not seen here, thereby confirming with XPS studies on the negligible presence of cobalt at the surface.

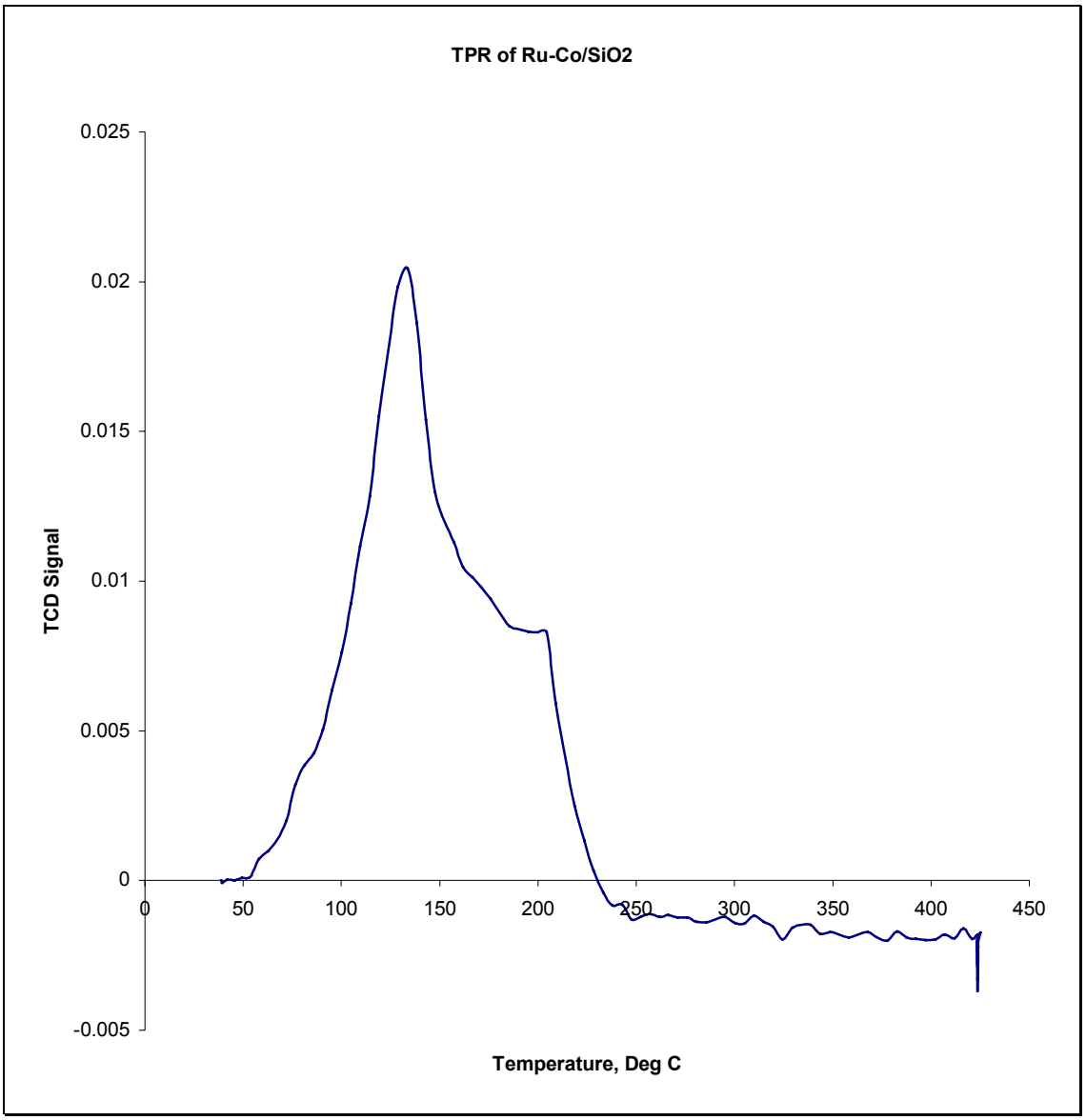

Figure 3.29 TPR of Ru-Co on SiO_2 support

CHAPTER IV

CONCLUSIONS

The use of bimetallic catalysts has gained growing importance in the field of heterogeneous catalysis over the past decade. This research has focused on the group VIII, IX and X elements, namely the bimetallic combinations of Pd, Rh, Ru on Co with silica support, which are common in hydrogenation studies of flue gases, in particular, the greenhouse gases. To better understand the structure and properties of these prepared bimetallic catalysts, characterization studies were done using the XPS, SEM-EDS, TPR and physisorption analysis. It was concluded that:

- Concentrations of Rh, Pd, Ru and Co at the surface were low, thereby suggesting low presence of metals at the surface, which was comprised mostly of silica support.
- Alloys and/or bimetallic particles for the three catalysts were not identified through the XPS and SEM results. However, the presence of bimetallic particles was confirmed for the Pd-Co and Ru-Co catalysts through the TPR results.

- In essence the elements present on the surface were identified, and all the metals were in the oxide state. The results of surface composition of metals were confirmed by SEM-EDS studies.
- XPS results showed only cobalt segregation, and the segregation of other metals was not clearly indicated but comparison of EDS and XPS results showed the surface segregation for rhodium, ruthenium and palladium as well.
- SEM micrographs did not reveal supporting information on the presence of alloys/and or bimetallic particles at the surface of the three catalysts.
- The physisorption analysis results for silica were in accordance with those of the manufacturer and are important parameters for bimetallic catalyst preparation methods employed in this research.

CHAPTER V

FUTURE STUDY

The current study talked about how successful we were in preparing these bimetallic catalysts by studying the formation of alloys and/or bimetallic particles, through the various surface characterization techniques described. A better understanding of this is possible by modifying the compositions of the catalysts and then comparing the results obtained with those of the current results.

Changing the atomic ratios of the metals with Co could change the surface properties of these bimetallic catalysts. It would be interesting to note the changes in the characteristic peaks observed through XPS, TPR and EDS. Additionally, any deviation from the results could give us a better indication of the alloys and/or bimetal particles formation. Reduction of these catalysts in H_2 prior to the experiments would eliminate or reduce the excess oxygen present thereby enhancing metal formation at the surface. The surface area and the percent metal dispersion are important factors that are to be determined; hence hydrogen chemisorptions studies could prove significant in the future studies. The final stages of our study would be the application of these bimetallic catalysts in the CO_2 hydrogenation reactions.

As these reactions proceed at high temperatures and pressures, it would be interesting to study the activity of these bimetallic catalysts and consequently towards methanol formation.

REFERENCES

[1] World Resources Institute website on Kyoto Protocol.www.wri.org/climate/kyoto.html [P.1]

[2] Song, Gaffney and Fujimoto, *" CO_2 Conversion and Utilization."* ACM Symposium Series 809 [P.3, 5, 8]

[3] EPA Global Warming site: National Emissions-Carbon Dioxide http://www.epa.gov/globalwarming/emissions/national/co2.html [P.5]

[4] U.S. Energy – related Greenhouse Gas Emissions website at http:// www.weathervane.rff.org/features/feature 123.htm [P.5]

[5] Table ES1 U.S. Emissions of greenhouse gases by gas, 1990-1998 http://www.eia.doe.gov/oiaf/1605/gg99rpt/tbles1.html [P.5]

[6] The Climate Problem http://www.igc.org/climate/ClimateProblem.html [P.5]

[7] The Climate Change Convention http://www.un.org/ecosocdev/geninfo/sustdev/climate.htm [P.5]

[8] BBC News/ SCI/TECH/Global warming 'could melt artic' http://news.bbc.co.uk/hi/english/sci/tech/newsid_1178000/1178764.stm [P.5]

[9] Harry Audus, Olav Kaarstad, Geoff Skinner, Greenhouse gas control technologies Conference paper, www.ieagreen.org.uk [P.7]

[10] Robyn Obert and Bakul C.Dave, "Enzymatic Conversion of Carbon Dioxide to Methanol: Enhanced Methanol Production in Silica Sol-Gel Matrices," *journal of American Chemical Society,* 121(51), 1999, pp. 12192-12193. [P.7]

[11] D.P.VanderWiel, J.l. Zilka-Marco, Y.Wang, A.Y.Tonkovich, R.S.Wegeng, "Carbon Dioxide Conversions in Micro reactors," *Pacific Northwest National Laboratory, Richland, WA 99352.* [P.7]

[12] Hiromi Yamashita, Akira Shiga, Shin-ichi Kawasaki, Yuichi Ichihashi, Shaw Ehara, and Masakazu Anpo, "Photo catalytic synthesis of CH4 and CH3OH from CO2 and H2O on highly dispersed active titanium oxide catalysts," *Energy Conservation Management,* Volume 36, No.6-9, 1995, pp. 617-620. [P.7]

[13] Hisao Hori,Osamu Ishitani, Kazuhide Koike, Frank P. A. Johnson, and Takashi Ibusuki,"Efficient carbon dioxide photoreduction by novel metal complexes and its reaction mechanisms, *"Energy Conversion Management,* Volume36, No.6-9, 1995, pp. 621-624. [P.7, 9, 15]

[14] Alfons Baiker, " Utilization of carbon dioxide in heterogeneous catalytic synthesis", *Applied Organometallic Chemistry,* 14,2000,pp. 751-762. [P.8, 9]

[15] M.Saito , T.Fujitani, I.Takahara, T.Watanabe, M.Takeuchi, Y.Kanai, K.Moriya, and T.Kakumoto, "Development of Cu/Zno- Based High Performance Catalysts for Methanol Synthesis by CO2 Hydrogenation," *Energy Conversion Management,* Volume36, No.6-9, 1995, pp.577-580. [P.9]

[16] Hitoshi Kusuma, Kiyomi Okabe, Hironori Arakawa, "Characterization of Rh-Co /SiO2 catalysts for CO2 hydrogenation with TEM, XPS and FT-IR," *Applied Catalysis A: General,* 207, (2001), pp. 85-94. [P.10, 25]

[17] A.Erhan Aksoylu et al., "Interaction between nickel and molybdenum in Ni-Mo/Al2O3 catalysts: CO2 methanation and SEM-TEM studies," *Applied Catalysis A: General,* 168 (1998), pp. 385-397. [P.10, 11]

[18] John H. Sinfelt, " *Catalysis: An old but continuing theme in Chemistry*," Exxon Research and Engineering Company. [P.10]

[19] Andreas Kogelbauer, James G. Goodwin, Jr., and Rachid Oukaci, "Ruthenium Promotion of Co/Al_2O_3 Fischer- Tropsch Catalysts," *Journal of Catalysis,* 160, 1996, pp.125-133. [P.13, 28]

[20] J.Kiviaho, M.K.Niemela, M. Reinikainen, T.A. Pakkanen, "TPR and FT-IR studies on carbonyl cluster derived Co-Ru /SiO_2 catalysts," *Applied Catalysis A: General,* 149, 1997, pp. 353-372. [P.13, 108]

[21] John H. Sinfelt, " *Bimetallic catalysts",* Exxon Research and Engineering Company. [P.14]

[22] Enrique Iglesia, Stuart L. Soled, Rocco A. Fiato, and Grayson H.Via, " Bimetallic Synergy in Cobalt-Ruthenium Fischer-Tropsch Synthesis Catalysts," *Journal of Catalysis,* 143, 1993, pp-345-368. [P.16]

[23] G.C.Bond, *"Heterogeneous Catalysis, Principles and Applications",* Second Edition, Oxford Science publications. [P.17, 18]

[24] W. Juszczyk, Z.Karpinski, D.Lomot, J.Pielaszek, Z.Paal and A.Yu.Stakheev, " The structure and activity of Silica Supported Palladium-Cobalt Alloys," *Journal of catalysis,* 142, 1993, pp. 617-629. [P.18, 104]

[25] Paul H. Emmet, "*Catalysis Volume 1, Fundamental Principles (Part 1*)," Reinhold Publishing Corporation. [P.23, 32]

[26] Operational manual of Adsorption by Quantachrome –Autosorb-1 [P.35]

[27] Barr, Terry Lynn, *"Modern ESCA: The Principles and practice of X-Ray Photoelectron Spectroscopy."* [P.36, 38]

[28] John F. Moulder, William F. Sticle, Peter E. Sobol and Kenneth D. Bomben, *" handbook of X-Ray Photoelectron spectroscopy",* a reference book of standard spectra for Identification and Interpretation of XPS data [P.36, 37]

[29] Automated Catalyst Characterization System manual by Autochem 2910-Micromeritics. [P.39, 43]

[30] S.Subramanian, "Temperature Programmed Reduction of Platinum Group Metals Catalysts," *Platinum Metals Rev.*, 36(2), 1992, pp.98-103. [P.39]

[31] Nicholas W. Hurst, Stephen J. Gentry, Alan Jones and Brian D. McNicol, "Temperature Programmed Reduction," *Catalysis Reviews,* - Science and Engineering, (24), 1982 [P.40, 41]

[32] Stanley L. Flegler, John W. Heckman, Jr., Karen L. Klomparens, " *Scanning and Transmission Electron Microscopy: An Introduction*," W.H.Freeman and Company, New York. [P.46]

[33] SEM-EDS lab, website http://www2.arnes.si/~sgszmera1/index.html [P.47]

[34] Feng-Shou Xiao, Atsushi Fukuoka, and Masaru Ichikawa, " Mechanism of Formation Oxygenated Compounds from $CO+H_2$ Reaction over SiO_2- Supported Ru-Co Bimetallic Carbonyl Cluster-Derived Catalysts," *Journal of Catalysis,* 138,1992, pp. 206-222. [P.60]

[35] Website for Surface Data for XPS from www.srdata.nist.gov [P.60]

[36] Jong Tae baek, hyung-Ho-Park, Kyung-Ik Cho, Hyung Joun Yoo, Sang Won Kang, and Byung Tae Ahn, " Interfacial reaction in the sputter-deposited $SiO_2/Ti_{0.1}W_{0.9}$ antifuse system," *Journal of Applied physics,* 78(12), 15 December 1995. [P.60]

[37] R.F.C Farrow, L.Folks, M.Toney, and S.A.Chambers, " MBE Growth and Magnetic Properties of Epitaxial Co Ferrite on MgO (001), *Interfacial Chemistry and Engineering 2000 Annual Report.* [P.64]

[38] Ana R. Ivanova, Guillermo Nuesca, Xiaomeng Chen, Cindy Goldberg, Alain E.Kaloyeros, Barry Arkles, and John J. Sullivan, " The Effects of Processing Parameters in the Chemical Vapor Deposition of Cobalt from Cobalt Tricarbonyl Nitrosyl", *Journal of The Electrochemical Society,* 146(6), 1999, pp.2139-2145. [P.64]

[39] Lucien Fiermans, Roger De Gryse, Greet De Doncker, Pierre A. Jacobs, and Johan A. Martens, " Pd Segregation to the surface of Bimetallic Pt-Pd Particles Supported on H-β Zeolite Evidenced with X-Ray Photoelectron Spectroscopy and Argon Cation Bombardment," *Journal of Catalysis,* 193, 2000, pp.108-114. [P.69]

[40] Yongfa Zhu, Li Zhang, Wenqing Yao, Lili CaO, " The chemical states and properties of doped TiO_2 film photocatalyst prepared using the Sol-Gel method with $TiCl_4$ as a precursor," *Applied Surface Science,* 158, 2000, pp.32-37. [P.69]

[41] M. Ono, K.Yoshii, T. Kuroki, N.Yamasaki, S.Tsunematsu and G.Bignall, "Development of Porous Silica Production by Hydrothermal Method," *High Pressure Research,* 20, 2001, pp.307-310 [P.70]

[42] L.Guczi, Z.Schay, G.Stefler, F.Mizukami, " Bimetallic catalysis: CO hydrogenation over palladium- cobalt catalysts prepared by sol/gel method," *Journal of Molecular Catalysis A: Chemical,* 141, 1999, pp.177-185. [P.68, 103, 104]

[43] H.F.J.Van'T blik, D.C.Koningsberger, and R.Prins, " Characterization of Supported Cobalt and Cobalt-Rhodium Catalysts," *Journal of Catalysis,* 97, 1986, pp. 210-218. [P.64, 106]

[44] L. Guczi, R. Sundarajan, Zs. Koppany, Z.Zsoldos, Z.Schay, F. Mizukami, and S. Niwa, " Structure and Characterization of Supported Ruthenium-Cobalt Bimetallic Catalysts," *Journal of Catalysis,* 167, (1997), pp.482-494. [P.108]